CHALMERS
UNIVERSITY OF TECHNOLOGY

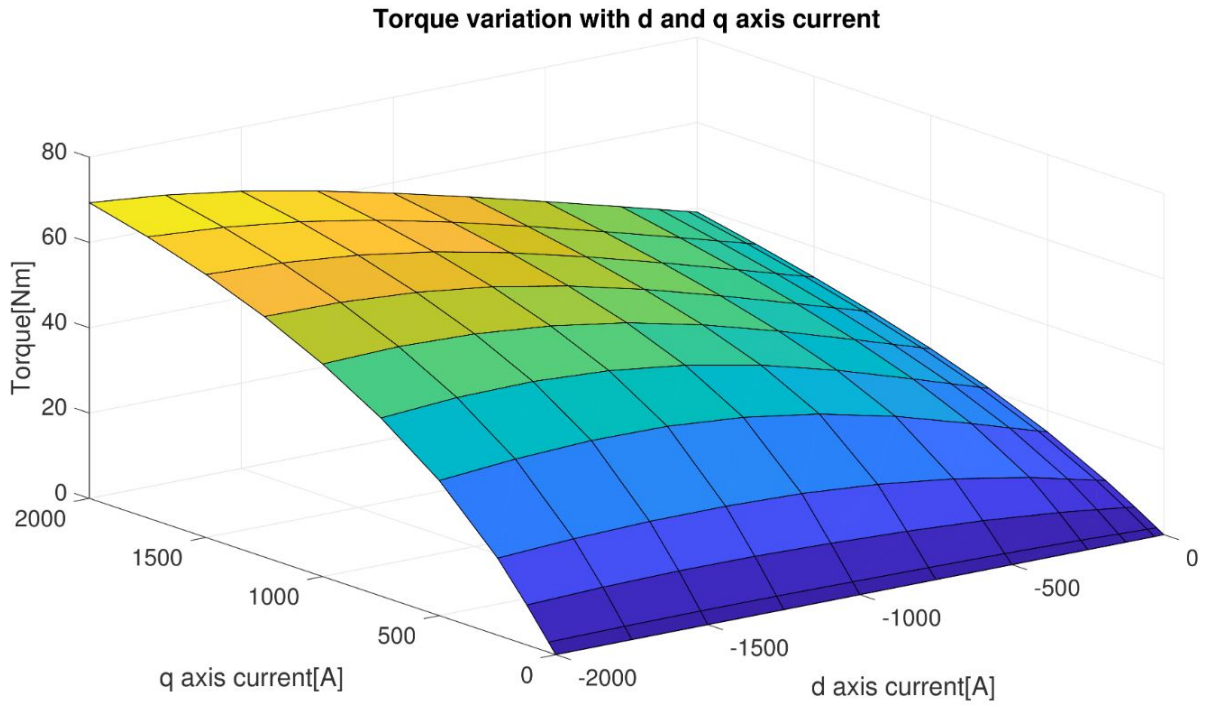

Extracting the maximum torque from a PMSM for a vehicular application by using different modulation techniques in the overmodulation region

Master's thesis in Electric Power Engineering

SHAYAN HALDER
XINGYUN YANG

Department of Electrical Engineering
CHALMERS UNIVERSITY OF TECHNOLOGY
Gothenburg, Sweden 2019

Master's thesis 2019

Extracting the maximum torque from a PMSM for a vehicular application by using different modulation techniques in the overmodulation region

SHAYAN HALDER
XINGYUN YANG

CHALMERS
UNIVERSITY OF TECHNOLOGY

Department of Electrical Engineering
Division of Electric Power Engineering
Chalmers University of Technology
Gothenburg, Sweden 2019

Extracting the maximum torque from a PMSM for a vehicular application by using different modulation techniques in the overmodulation region
SHAYAN HALDER
XINGYUN YANG

Supervisor: Torbjörn Thiringer, Electric Power Engineering
Taiye Adeboye, Volvo Car Corporation
Torbjörn Larsson,Volvo Car Corporation

Examiner: Torbjörn Thiringer, Electric Power Engineering

Master's Thesis 2019
Department of Electrical Engineering
Division of Electric Power Engineering
Chalmers University of Technology
SE-412 96 Gothenburg
Telephone +46 31 772 1000

Abstract

In this thesis, three different modulation techniques are analysed in the region of overmodulation. The three different techniques analysed are classical Overmodulation(covm), space vector modulation(svm) and discontinuous modulation with 60 degree clamping(dpwm1). The aim is to extend the operation of the aforementioned modulation techniques to their maximum limit. The performance of the modulator and their effects on an electric machine and its performance are analysed. The key parameters analysed are average torque, machine losses(Copper loss and iron loss), current thd, voltage thd, switching loss and conduction loss.

Different modulation techniques exhibit different capabilities of realising fundamental voltages. DPWM with 60 degree clamp was found to have a higher fundamental voltage when compared to any other modulation technique. The operating points selected are located in the flux weakening region of the machine, where the voltage dependency exists. A steady state control algorithm has been devised to generate the necessary parameters which are then fed to the finite element modelling package Ansys Maxwell to analyse the average torque and machine loss consequences.

The operating points used are 12000 rpm and 20000 rpm, the torque values selected are the maximum torques that can be obtained from the machine at these speeds respectively. The average torque for increase for covm, svm, dpwm0 and dpwm1 are 12.02%, 12.02%, 12.56% and 13.7% respectively at 20000 rpm, whereas at 12000 rpm the increase was found to be 10% for dpwm1 and 9% for covm. In terms of machine losses, especially in case of iron losses, the increase was 7.16% for dpwm1 and 8.3% for covm, 3.65% for dpwm1, 4.6% for covm, 4.09% for svm, 3.96% for dpwm0, at speeds 12000 rpm and 20000 rpm respectively. The same trend was observed for the current thd.

In terms of inverter loss analysis, it was found that for the same modulation index the magnitude of loss was higher in case of covm than dpwm1, which in turn corresponds to higher inverter working efficiency. In terms of voltage thd it was seen that with the increase in modulation index, the voltage thd dropped and was found to be the least at 6 step operation.

Keywords: Modulation technique, SVM, dpwm1, covm , FEM, iron loss, inverter, losses, efficiency.

Acknowledgements

This thesis is conducted at Volvo Cars Corporation and the department of Electric Power Engineering at Chalmers University of Technology.

First of all, we would like to express our gratitude to our supervisor as well as our examiner, Prof. Torbjörn Thiringer who gave us the opportunity to do this wonderful thesis work. Any attempt at any level can 't be satisfactorily completed without the care, support and guidance from him.

We also would like to thank our supervisors at Volvo Cars, Adeboye Taiye and Torbjörn Larsson for their time and contributions.

Many people, both at Volvo Cars and Chalmers have been involved to varying degrees and support. We would like to thank them all, especially Stefan Skoog for his help in FEM simulations and Chengjung Tang for his help with space vector modulation.

Finally, we would like to express our deepest love to our parents for supporting us along the way.

Shayan Halder, Xingyun Yang, Gothenburg, August 2018

1
Introduction

1.1 Background

High performance of electric machines is of vital importance for an electric vehicles(EV) and for a hybrid electric vehicles(HEV). The control of the permanent magnet synchronous machines (PMSM) itself has been fully developed nowadays, however the influence of the power converter control system is lacking in previous studies, especially the modulation techniques which may have a large influence on the inverter performance. Different modulation techniques need to be investigated and compared in order to maximize motor performance in a vehicle application.

1.2 Goal

The goal of this thesis work is to quantify the possible extra power that can be extracted from a PMSM-drive, by using various modulation techniques, such as classical overmodulation, space vector modulation and discontinous pulse width modulation(PWM). Furthermore the negative effects such as harmonics and losses need to be compared regarding different modulation techniques.

1.3 Outline

The outline of this thesis is as follows. In section 2, modeling and control of a PMSM drive system, different modulation strategies and performance evaluations like machine losses, inverter losses and harmonics are presented. In section 3, the modulation techniques which have been discussed in section 2 are implemented and the switching patterns are shown. In section 4, simulation results are shown and analyzed in detail. Finally, section 5 presents the conclusion of thesis work.

2
Theory

2.1 Electric Machine modelling and Control

Electric machine control is a well-developed and popular research area. In the automotive industry where an electrical machine is supposed to operate at constant power for a more extensive speed range, a salient pole interior mounted permanent magnet synchronous machine(SP-IPMSM) is found to be advantageous. A permanent magnet synchronous machine(PMSM) has more reliability than Direct current(DC) machines because of no commutator and is more efficient than an Induction Machine(IM) as permanent magnets aid the production of rotor flux. To extract high performance from an electric machine, different control techniques have been developed and implemented. Two of the most popular technique are Field Oriented Control(FOC),and Direct Torque Control(DTC) [1].

Among the above two types of control methods, FOC is generally used for high-performance drive systems. This type of control technique is a closed loop control. It uses rotor angle as feedback from the speed sensor. Besides this, it also uses a current controller to dynamically control currents, thereby controlling electromagnetic torque and flux in the machine. The main advantages of this method being transformation of a complex and coupled AC model into a linear system, independant control of torque and flux, fast dynamic response, excellent transient and steady-state performance, high torque and low current during startup, high efficiency, wide speed range through field weakening. The main disadvantages are that this method is costly, it also needs a modulation algorithm to be used with the inverter.

The DTC method works without any speed feedback; it uses advanced machine theory to determine motor torque directly. The two variables in this control method are motor torque and flux linkage[ABB].In this technique, an appropriate voltage vector is applied by switching the inverter from a pre-defined switching table. The advantages of this method are faster torque response than FOC. The disadvantage of this control method is that when applied on PMSM, the rotor feedback is necessary.

2.1.1 PMSM modelling and Control

A PMSM is generally constructed with sinusoidally distributed windings, with a 120° phase difference between the three phases. In a stator reference frame coordinate system the phase vectors A, B, C can be seen as they are 120° separated in angle, but with time-varying amplitude [2]. This three vector representation for calculating the machine parameters is too complex, and the analysis of the machine model could become much easier by transforming the system into a two vector orthogonal system, both in steady state and dynamic state. The transformation of the 3 phase system to the stationary reference frame is done using Clarke transformation and the change of coordinates from the stationary reference frame to the synchronous reference frame is done using park transformation.The different transformations are shown in fig 2.1, where i_a,i_b and i_c are the currents in 3 phase system and ω is the angular speed of the resultant magneto-motive force denoted as F, similarly i_α,i_β,i_d and i_q are the currents in stationary reference frame and synchronous reference frame respectively.

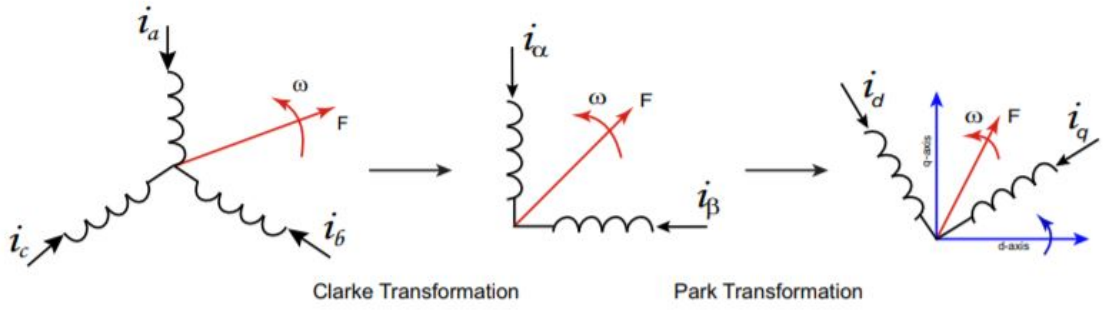

Figure 2.1: Coordinate transformations from 3 phase to alpha-beta and dq .

2.1.2 Equivalent circuit model

The mathematical model of an SP-PMSM in synchronously rotating reference frame can be represented as equivalent circuits as shown in fig 2.2. This figure shows PMSM model in the DQ reference frame, where R_s is the stator resistance,L_{sd} and L_{sq} are the inductances along d and q axis respectively, ω_r is the synchronous electrical speed at which the rotor is rotating, i_{sd} and i_{sq} are the current in DQ frame and Ψ_m is the flux linkage from permanent magnets..The control of a PMSM is preferably done in the DQ reference frame since it is easy to tune the controller[3].

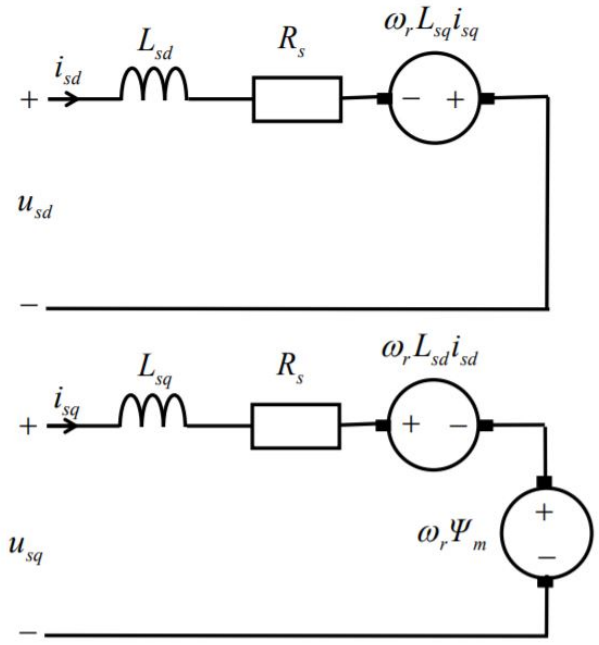

Figure 2.2: Equivalent circuit model of PMSM in synchronous reference frame .

The stator equations corresponding to fig 2.2 are expressed as

$$u_{sd} = R_s i_{sd} + L_{sd}\frac{di_{sd}}{dt} - \omega_r L_{sq} i_{sq} \tag{2.1}$$

$$u_{sq} = R_s i_{sq} + L_{sq}\frac{di_{sq}}{dt} + \omega_r L_{sd} i_{sd} + \omega_r \Psi_m \tag{2.2}$$

The flux linkage in a SP-PMSM in terms of inductance and current can be defined as

$$\Psi_d = L_{sd} i_{sd} + \Psi_m \tag{2.3}$$

$$\Psi_q = L_{sq} i_{sq} \tag{2.4}$$

Torque equation in a SP-PMSM can be expressed in terms of the current and flux linkage as [4]

$$T_{em} = \frac{3np}{2}(\psi_d i_{sq} - \psi_q i_{sd}) \tag{2.5}$$

where np is number of pole pairs of the rotor. Substituting (2.3), (2.4) and (2.5), the electromagnetic torque can be expanded as

$$T_{em} = \frac{3np}{2}((L_{sd} - L_{sq}) i_{sd} i_{sq} + \psi_m i_{sq}) \tag{2.6}$$

The first term in (4.6) is termed as reluctance torque which is unique in SP-PMSM and the second term is the torque due to permanent magnets. Therefore the total electromagnetic torque can be expressed as

$$T_{em} = T_{rel} + T_{pm} \tag{2.7}$$

where T_{rel} is the reluctance torque and T_{pm} is the torque produced by the permanent magnets.

In the discussed model the variation in L_{sd}, L_{sq} and ψ_m are not considered. These variations generally depend upon i_{sd}, i_{sq} and magnetic saturation of iron in an electric machine.

2.1.3 Field oriented control of PMSM

The FOC control method consists of a speed controller on the outer loop and an inner current controller. The controller design is done using internal model control(IMC) strategy [5]. The aim of this strategy is to have in-dependant control over the torque and the magnetic field in the machine. This is implemented using two control loops

- The outer speed loop which generates the reference torque[1].
- The inner current controller loop which controls the flux and the torque from the stator side[1].

The information of the three-phase stator currents, the DC link voltage and the position of the rotor is required to execute the FOC control method. In this control scheme, the three phase currents and the rotor speed are sampled based on an interrupt generated by the digital controller. The speed obtained is then integrated to determine the rotor position. Using Clarke's transformation the currents from the three-phase reference frame are transformed into orthogonal stationary reference frame, another transformation known as Park's transformation is used to convert this orthogonal stationary reference frame into a synchronously rotating reference frame. The feedback from the speed controller is generally sensed by a speed sensor commonly known as resolver or encoder. This is fed as an input to the speed control block which then generates torque reference, and This information is used to determine the current references which are tracked by the current controller. The current controller consists of proportional and integral control for each of the d and q axis currents independently. The current controller generates a voltage in a synchronously rotating reference frame which is then converted to three phase reference frame by using inverse Park and inverse Clarke transformations. This resulting voltage is then applied as a reference to the modulator to generate timing signals. These timing signals determines the duty cycle of the different switches of the inverter that feeds the electric machine [1].

2.1.4 Control Algorithms for the Electric Drivesystem

2.1.4.1 MTPA

The maximum torque per ampere(MTPA) is a control strategy used in electric machines, where the minimum current is applied to the machine to produce a particular torque.This strategy improves the efficiency as it aids in minimizing losses in the form of copper loss.

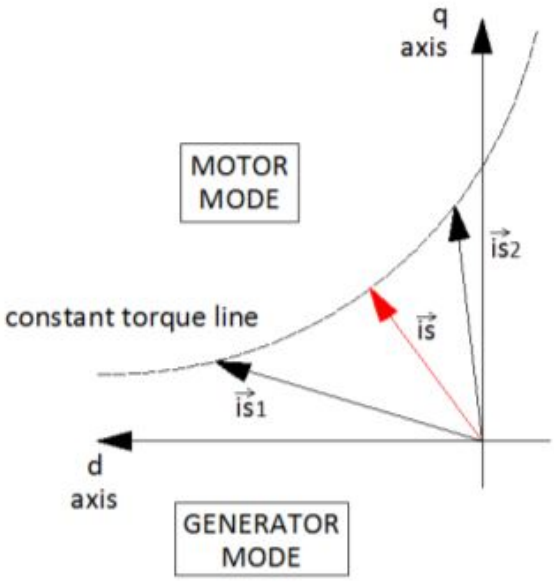

Figure 2.3: Equivalent circuit model of PMSM in synchronous reference frame [1]
.

For a certain torque reference, there are numerous combinations of stator current vectors i_{sd} and i_{sq} that can produce the required torque, but only one combination produces minimum current which results in least copper losses, which is evident from the I_s vector in figure 2.3. The MTPA trajectory can be obtained by using the torque equation in (2.6). To determine the MTPA curve a current constraint needs to be added, which is generally dictated by the physical current limitation of the inverter.

$$I_{smax}^2 <= I_{sd}^2 + I_{sq}^2 \tag{2.8}$$

where I_{sd} and I_{sq} are the d and q axis stator currents respectively. I_{smax} is the maximum stator current capability of the inverter. To solve for the optimum current angle β, The d and q axis currents are re-written in terms of the current angle as

$$I_{sd} = I_{smax} cos(\beta) \tag{2.9}$$

$$I_{sq} = I_{smax} sin(\beta) \tag{2.10}$$

The substituition of (2.9) and (2.10) in the torque equation(2.6) leads to

$$T_{em}(\beta) = 1.5 * n_p(\Psi_m I_{smax} sin(\beta) + (L_{sd} - L_{sq}) I_{smax}^2 sin(\beta) cos(\beta)) \tag{2.11}$$

The equation(2.11) is differentiated with respect to β and then equated to zero to obtain the maximum of the torque function.The expression for current angle β is as follows

$$cos(\beta) = -\frac{\Psi_m}{4(L_{sd} - L_{sq}) I_{smax}} - \sqrt{0.5 + (\frac{\Psi_m}{4(L_{sd} - L_{sq}) I_{smax}})^2} \tag{2.12}$$

Using the obtained value of current angle β the minimum d and q axis currents can be determined for the desired torque level. It is to be noted that this is a simplified approach to MTPA and doesn't include L_{sd} and L_{sq} saturation. In this work, a nonlinear algorithm is used to be able to include the phenomena of saturation.

2.1.4.2 Field Weakening

This is a application specific control as this needs the electric machine to be operated at speeds higher than the base speed of the machine. At the end of MTPA, when the current trajectory has reached both the voltage and the current limit of the inverter, then the only way of operating the machine at extended speed is flux weakening. This is conducted by injecting more negative d-axis current, which in turn results in reducing the net flux, so the net voltage in q direction is therefore reduced[1]. When executing this type of control, voltage, and current constraints need to be implemented. The maximum voltage limit is set in accordance with the maximum voltage capability of the inverter, and the current limitation is the same as (2.8). The Voltage constraint can be expressed as

$$U_{smax}^2 <= U_{sd}^2 + U_{sq}^2 \tag{2.13}$$

where U_{smax} is the maximum phase voltage that the inverter is capable of providing. Referring to the d and q axis voltage equations i.e (2.1) and (2.2), at very high speeds, the stator resistance can be ignored and therefore the equation is modified to

$$u_{sd} = L_{sd}\frac{di_{sd}}{dt} - \omega_r L_{sq} i_{sq} \tag{2.14}$$

$$u_{sq} = L_{sq}\frac{di_{sq}}{dt} + \omega_r L_{sd} i_{sd} + \omega_r \Psi_m \tag{2.15}$$

The following expression could be written by substituting (2.14) and (2.15) in the voltage constraint (2.13) and ignoring the dynamic states.

$$(\frac{U_{smax}}{w_r})^2 >= L_{sd}(\frac{\Psi_m}{L_{sd}} + i_{sd}) + (L_{sq} i_{sq}) \tag{2.16}$$

The equation(2.16) represents an ellipse with centre located at $(-\frac{\Psi_m}{L_{sd}}, 0)$, this point also decides if a drive is a finite speed drive or a infinite speed drive. This point represents the stator current at which the rotor speed is having theoretical infinite speed. It can also be deduced from the ellipse equation that with increasing speed the ellipse starts to collapse to its centre [1].

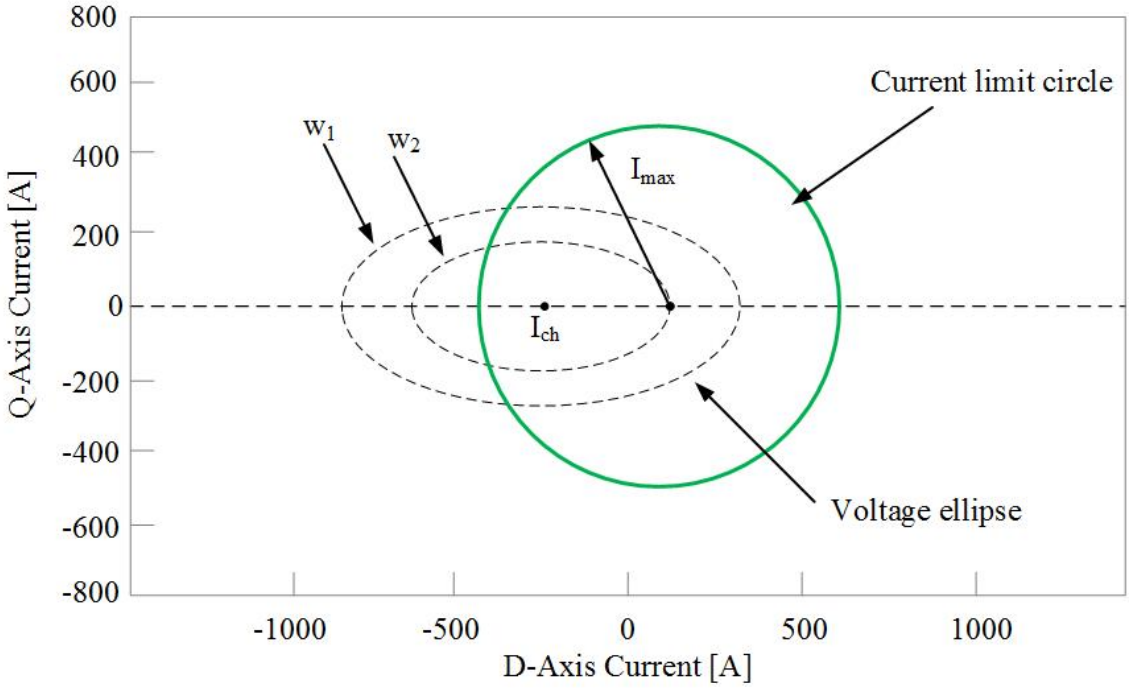

Figure 2.4: Voltage ellipse and current limit circle .

The figure(2.4) illustrates the current limit constraint in the form a circle, and the ellipse is seen to be decreasing from w1 to w2, which indicates that speed w1>w2. The field weakening current references are obtained on the intersection points of the current limit circle and the consequently occurring voltage ellipse. Therefore it is evident that in field weakening the available torque from the machine is a function of the speed.

2.1.4.3 MTPV

With a further increase of the machine speed, the voltage ellipse will fall into the maximum current circle which means that the maximum current cannot be maintained anymore, a control strategy of maximum torque per volt(MTPV) will instead by applied. The analytical approach to MTPV control strategy is discussed in this section. (2.3) and (2.4) can be rearranged to form the stator currents in d and q domain in terms of flux linkages as follows

$$I_{sd} = \frac{\Psi_d - \Psi_m}{L_{sd}} \tag{2.17}$$

$$I_{sq} = \frac{\Psi_q}{L_{sq}} \tag{2.18}$$

The stator flux linkage magnitude is defined as

$$\Psi_s = \sqrt{\Psi_d^2 + \Psi_q^2} \tag{2.19}$$

where Ψ_d and Ψ_q are the flux linkages in the d and q directions respectively. By neglecting the resistive voltage drop components and the dynamic terms in (2.14)

and (2.15), the stator voltage equations can be rewritten as

$$u_{sd} = -\omega_r L_{sq} I_{sq} \tag{2.20}$$

$$u_{sq} = \omega_r L_{sd} I_{sd} + \omega_r \Psi_m \tag{2.21}$$

Combining (2.20) and (2.21),

$$U_{smax}^2 = \omega_r^2 (L_{sq} I_{sq})^2 + \omega_r^2 (L_{sd} I_{sd} + \Psi_m)^2 \tag{2.22}$$

Rearranging the following equation can be framed

$$\frac{U_{smax}^2}{\omega_r^2} = (L_{sq} I_{sq})^2 + (L_{sd} I_{sd} + \Psi_m)^2 \tag{2.23}$$

The stator flux linkage in terms of stator voltage now takes the form

$$\Psi_s = \frac{U_{smax}}{\omega_r} \tag{2.24}$$

The currents can now be written in terms of flux linkages as

$$I_{sq} = \sqrt{\frac{\frac{U_{smax}^2}{\omega_r^2} - \Psi_d^2}{L_{sq}^2}} \tag{2.25}$$

The equations determined in the process can now be used to derive the torque equation in terms of stator flux linkage and d axis flux linkage

$$T_{em} = 1.5 n_p [\Psi_d (\frac{\sqrt{\Psi_s^2 - \Psi_d^2}}{L_{sq}}) + \sqrt{\Psi_s^2 - \Psi_d^2} (\frac{\Psi_m - \Psi_d}{L_{sd}})] \tag{2.26}$$

This torque equation which is a function of flux linkage in d axis can now be maximized by differentiating it with respect to d axis flux linkage and equating it to zero. Post maximization the following equation can be obtained for Ψ_d

$$\Psi_d = \frac{-L_{sq}\Psi_m + \sqrt{(L_{sq}\Psi_m)^2 + 8(L_{sd} - L_{sq})^2 \frac{U_{smax}}{\omega_r}^2}}{4(L_{sd} - L_{sq})} \tag{2.27}$$

Now (2.17) and (2.25) can be used to determine the reference currents in this region of operation. It is to be noted that if the characteristic current lies inside the current circle, this control algorithm can be utilized. This strategy extends the operating speed but reduces torque as the trajectory leaves the current circle as can be seen from figure 2.5 and therefore, the maximum current can no longer be utilized.

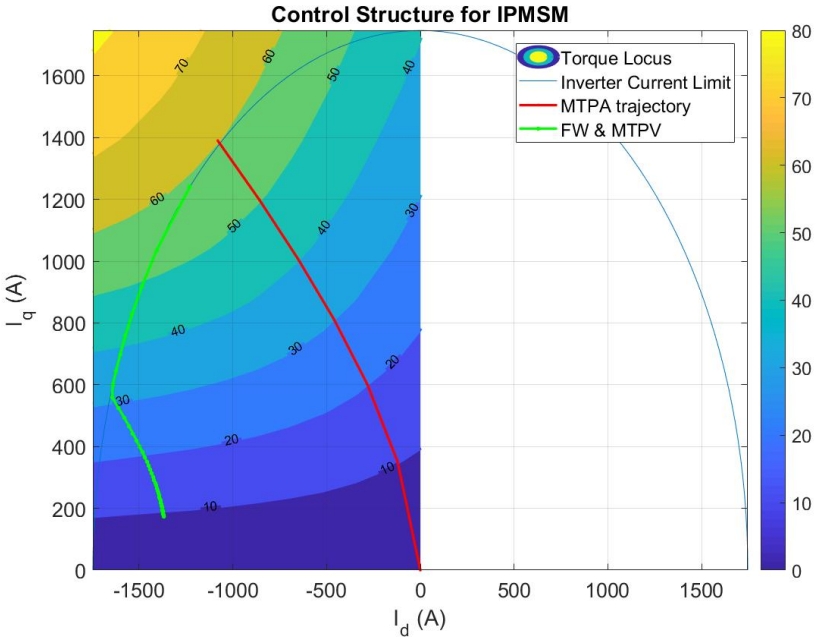

Figure 2.5: Control Structure of IPMSM in FOC .

Figure 2.5 illustrates the different trajectories in the control of IPMSM in FOC. The line marked in red shows the MTPA trajectory with the inclusion of inductance saturation. In the region of high-speed operation, the path followed is the green line which includes both Field Weakening and MTPV. The endpoint of the trajectory defines the infinite speed point, and current at that point is also termed as characteristic current.

2.2 Modulation strategies

2.2.1 Modulation

An inverter produces an AC output voltage from a DC link through a modulator by comparing the sinusoidal reference analog signal with a periodic waveform, called the carrier signal as shown in figure 2.6.

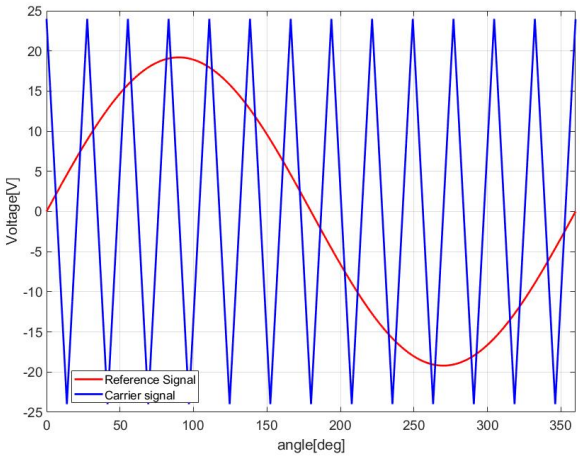

Figure 2.6: Modulation reference signal and carrier signal.

For a certain inverter phase, if the reference signal is larger than the carrier signal, the corresponding upper switch is on, otherwise it's off and the lower switch is on, the resulting output voltage waveform is therefore a digital pulse width pattern which is shown in figure 2.7, the fundamental component of the output voltage is still a sinusoidal wave.

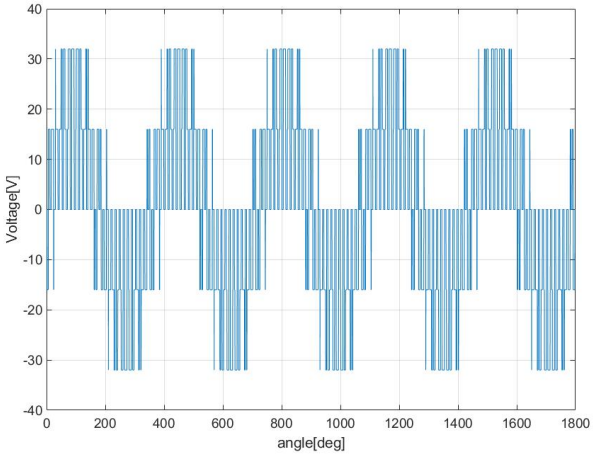

Figure 2.7: Output voltage pattern after modulation.

2.2.2 Overmodulation

The area of operation from loss of linear control to complete loss of control of voltage is termed as overmodulation [6]. For a carrier-based modulation strategy, overmodulation occurs when the reference signal is higher in magnitude than the high-frequency carrier. The switching ceases for that particular point of time, and the signal becomes clamped to the upper or lower DC bus as is demonstrated in figure 2.8, the consequent switching pattern is as shown in figure 2.9. In the case of third harmonic injection into the reference voltage, the fundamental magnitude of the output voltage is increased by injecting a third harmonic component, the advantage of this injection is that the linear control of voltage is not lost. This facilitates better utilization of the inverter's DC link. But the voltage margin can be increased further by letting the modulator overmodulate. The modulator partly loses control of the waveform, especially in areas where it saturates. This type of technique also means that low order frequency harmonic components around the fundamental appear, which leads to waveform distortion. The worst case of overmodulation is a 6 step operation. As explained in [6] the process of pulse dropping is termed as overmodulation.

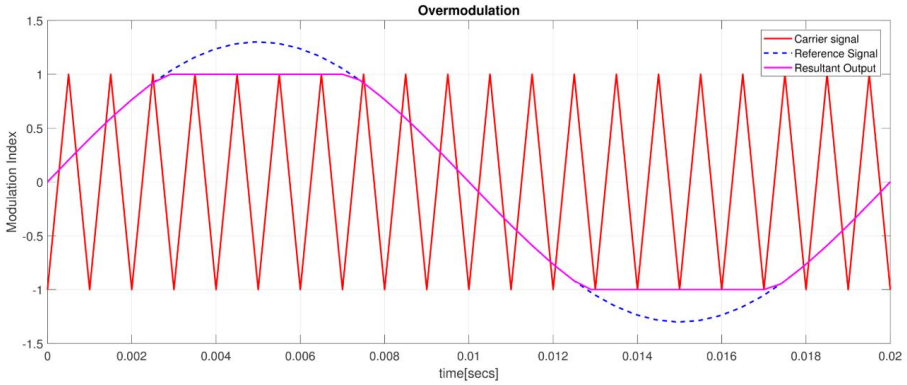

Figure 2.8: Overmodulated reference signal .

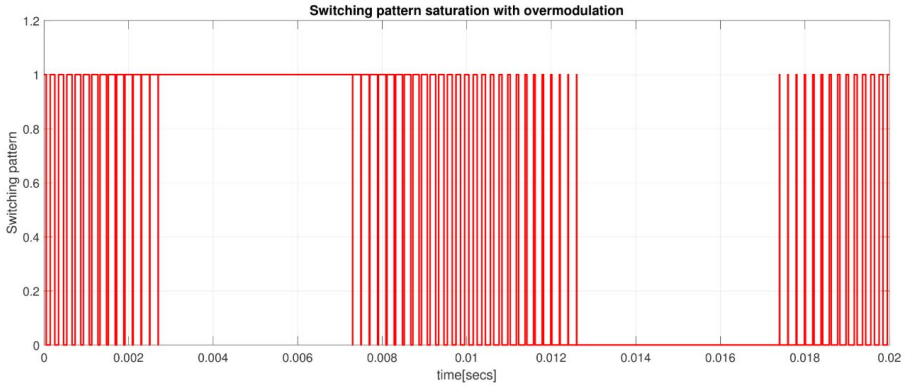

Figure 2.9: Switching pattern for overmodulation .

In case of overmodulation an effective modulation index and a gain index is defined which are the ratio of the modulating signal fundamental to $\frac{U_{dc}}{2}$ and the ratio of

effective modulation index to the modulation index defined in (2.28) respectively [7]. The purpose of such a performance parameter aids in determining when the fundamental of the output phase voltage from the inverter saturates. The definition of modulation index used in this work is

$$MI = \frac{U_{fundamental}}{\frac{U_{dc}}{2}} \tag{2.28}$$

Where MI is the modulation index and $U_{fundamental}$ is the fundamental component of the modulating signal. It is to be noted that with increase in modulation index the effective modulation index increases as it is the linear modulation region, which is a modulation index of 1.155, MI greater than 1.155 is in region I of overmodulation and any value of MI greater than 1.333 is in region II of overmodulation, further increase in MI would result in pure 6-step operation.

2.2.3 Classical Overmodulation

Classical overmodulation(COVM) is defined as the modulation technique where sinusoidal reference voltages which are phase shifted by 120° are injected with a zero sequence component determined in the following way

$$V_{max} = max[V_{refa}, V_{refb}, V_{refc}] \tag{2.29}$$

$$V_{min} = min[V_{refa}, V_{refb}, V_{refc}] \tag{2.30}$$

$$V_{cm} = \frac{1}{2}(V_{max} + V_{min}) \tag{2.31}$$

The COVM waveform for phase A can then be determined by

$$V_{refa} = V_m sin(\omega t + \phi) - V_{cm} \tag{2.32}$$

Where V_{cm} is the appropriate common mode voltage that should be injected to obtain the desired waveform demonstrated in the fig 3.4 and 2.11.It can be observed that the COVM waveform is a saddle-shaped waveform with a fundamental that is almost 15.5% higher than a sinusoidal signal without common mode injection. Classical overmodulation occurs when the saddle-shaped waveform peak has a modulation index greater than $+\frac{U_{dc}}{2}$ or less than $-\frac{U_{dc}}{2}$. The voltage would result in 6 step for a modulation index of 2.3094.

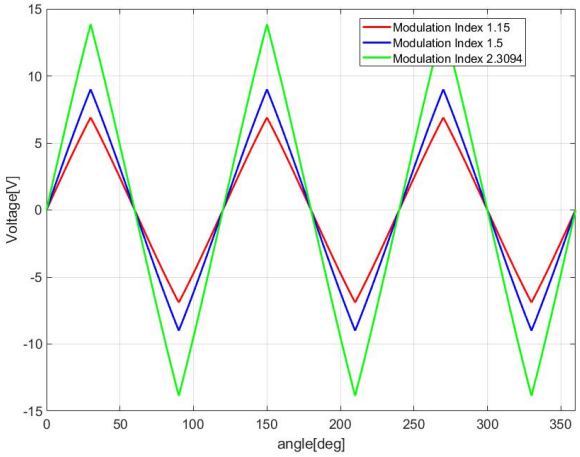

Figure 2.10: Common mode waveform COVM .

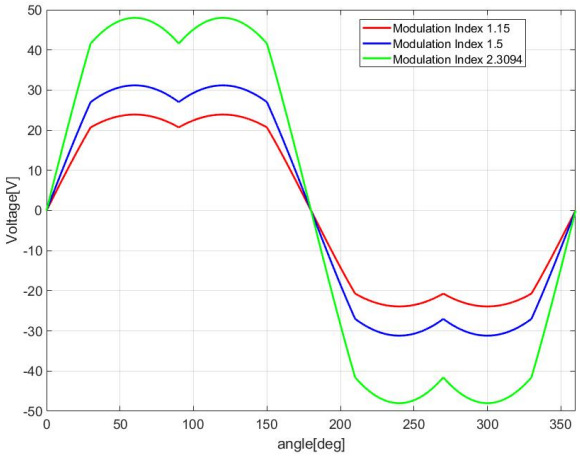

Figure 2.11: Classical Over-modulation with zero sequence injection .

2.2.4 Space Vector Modulation

The main idea of space vector modulation(SVM) is using different switching combinations to get a quasi-circular rotating voltage vector[6].
As shown in Fig.2.12, a two level three phase has six switches $s_a, s_b, s_c, s'_a, s'_b, s'_c$. Define switching state 1 as switch on and 0 as switch off, if the upper switch is on then the lower switch should be off, therefore only three upper switches' case need to be considered. There are eight possible switching states where all three switches on and all three switch off results in a short circuit of the output voltage, so these two vectors are named as zero vector. And the other six switching combinations could compose a set of voltage space vectors with the same amplitude of $2U_{dc}/3$ but different phase, therefore these six vectors are named as active vector. The output voltage vector could be expressed using the switching state as

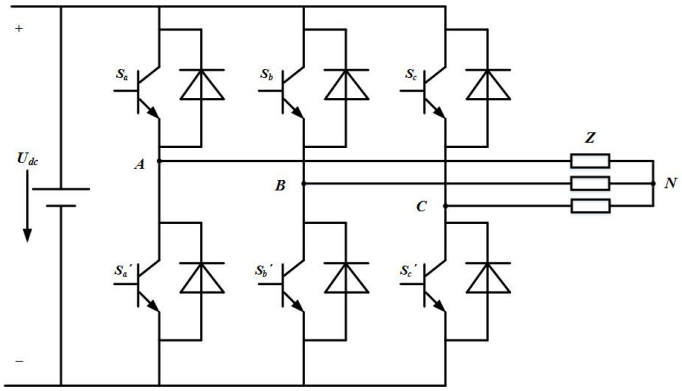

Figure 2.12: Inverter model for SVM.

$$U_{out} = \frac{2U_{dc}}{3}(s_a + s_b e^{j\frac{2}{3}\pi} + s_c e^{-j\frac{2}{3}\pi}) \tag{2.33}$$

Besides, the AC side phase voltage V_{AN}, V_{BN} and V_{CN} could be expressed as

$$\begin{cases} V_{AN} = \frac{U_{dc}}{3}(2s_a - s_b - s_c) \\ V_{BN} = \frac{U_{dc}}{3}(2s_b - s_a - s_c) \\ V_{CN} = \frac{U_{dc}}{3}(2s_c - s_a - s_b) \end{cases} \tag{2.34}$$

By inserting the eight switch combination into (2.34), values of the phase voltage, line voltage and U_{out} can be obtained as shown in Table.2.1

Table 2.1: Switching combination and voltage.

s_a	s_b	s_c	V_{AN}	V_{BN}	V_{CN}	V_{AB}	V_{BC}	V_{CA}	U_{out}
0	0	0	0	0	0	0	0	0	0
1	0	0	$2U_{dc}/3$	$-U_{dc}/3$	$-U_{dc}/3$	U_{dc}	0	$-U_{dc}$	$2U_{dc}/3$
0	1	0	$-U_{dc}/3$	$2U_{dc}/3$	$-U_{dc}/3$	$-U_{dc}$	U_{dc}	0	$2U_{dc}/3e^{j\frac{2\pi}{3}}$
1	1	0	$U_{dc}/3$	$U_{dc}/3$	$-2U_{dc}/3$	0	U_{dc}	$-U_{dc}$	$2U_{dc}/3e^{j\frac{\pi}{3}}$
0	0	1	$-U_{dc}/3$	$-U_{dc}/3$	$2U_{dc}/3$	0	$-U_{dc}$	U_{dc}	$2U_{dc}/3e^{j\frac{4\pi}{3}}$
1	0	0	$U_{dc}/3$	$-2U_{dc}/3$	$U_{dc}/3$	U_{dc}	$-U_{dc}$	0	$2U_{dc}/3e^{j\frac{5\pi}{3}}$
0	1	1	$-2U_{dc}/3$	$U_{dc}/3$	$U_{dc}/3$	$-U_{dc}$	0	U_{dc}	$2U_{dc}/3e^{j\pi}$
1	1	1	0	0	0	0	0	0	0

As mentioned before, the switching combinations lead to six active voltage vector and two zero voltage vectors which could be reflected into a complex plane as shown in Fig.2.13, the complex plane is therefore divided into six sectors, each sector contains two active voltage vectors which value is equal to $2U_{dc}/3$. For linear modulation, any required voltage can be achieved, i.e. the output voltage U_o is equal to the reference voltage U_{ref}.

$$\begin{cases} |U_{ref}|sin\alpha T_s = |U_6|sin60°T_1 \\ cos\alpha T_s = |U_4|T_2 + |U_6|cos60°T_1 \end{cases} \tag{2.35}$$

According to voltage second balance equation (2.35), the reference voltage U_{ref} can be achieved by applying a certain time T_1 and T_2 on the two active vectors respectively as well as the rest of one switching period T_0 on zero vectors as shown in

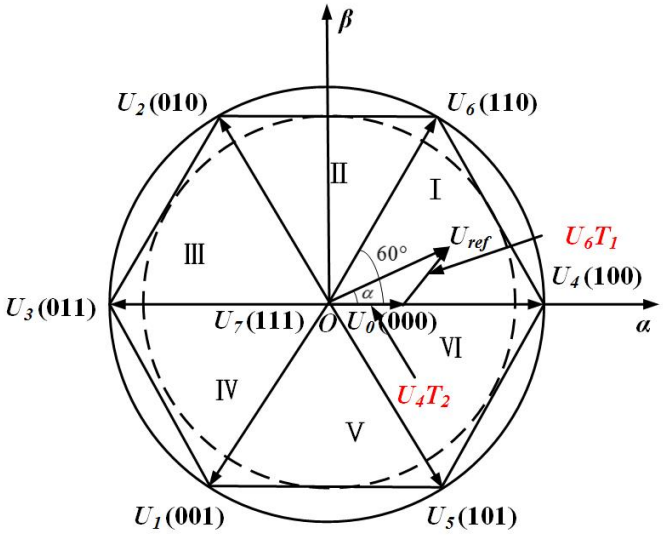

Figure 2.13: Voltage space vector in a complex plane.

Fig.2.13, which trajectory follows a circle. The total applied time during one switching period follows the rule $T_1 + T_2 + T_0 = T_s$ where T_s is switching period. Since zero vector does not produce any voltage, the only effective time is $T_1 + T_2$. The longer the effective time applied, the more voltage can be achieved. The maximum available time $T_1 + T_2$ is one switching period T_s.

When reference voltage is larger than $U_{dc}/\sqrt{(3)}$(overmodulation), the reference voltage cannot be fully achieved[8]. Overmodulation for space vector modulation can be divided into two regions. Take sector 1 as an example, region 1 as shown in Fig2.14,

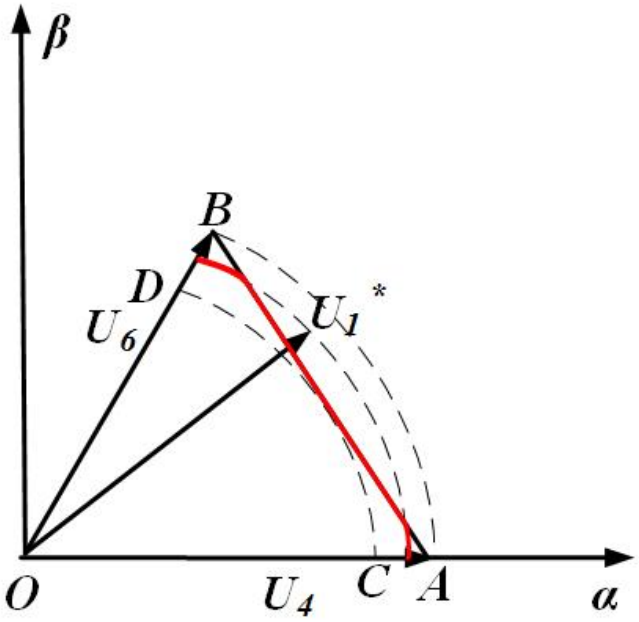

Figure 2.14: Space vector overmodulation region 1.

is between the inner tangential circle CD and the circumscribed circle AB where the reference voltage is between $U_{dc}/\sqrt{(3)}$ and $2U_{dc}/3$. For reference voltage which is outside line AB, $T_1 + T_2$ is larger than T_s, so the applied time has to be linearly reduced by the following equation.

$$\begin{cases} T_1 = \frac{T_1}{T_1+T_2} T_s \\ T_2 = \frac{T_2}{T_1+T_2} T_s \end{cases} \tag{2.36}$$

The output voltage is thus smaller than the reference voltage, the actual output voltage trajectory follows the red line.

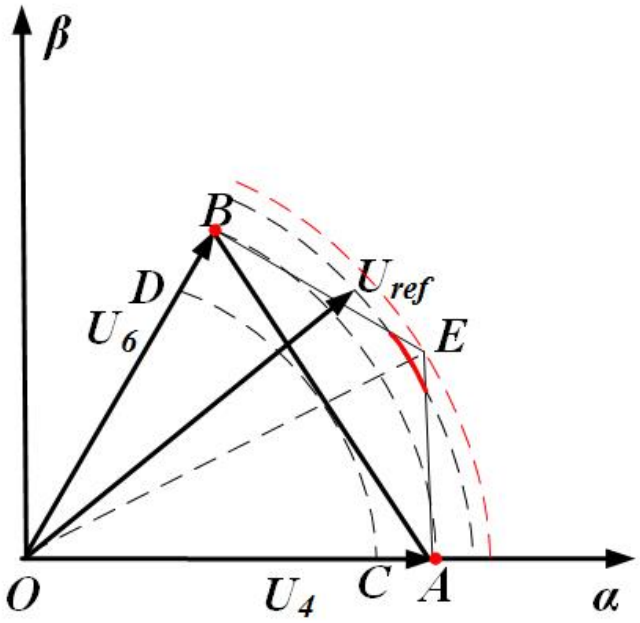

Figure 2.15: Space vector overmodulation region 2.

Region 2 as shown in Fig. 2.15, is outside the circumscribed circle AB where reference voltage is larger than $2U_{dc}/3$. If the reference voltage falls within triangle OAE or OBE, the applied time is linearly reduced similarly as for region 1, the actual output voltage trajectory follows the red line, otherwise the actual output voltage stays in line OA or OB. When reference voltage achieves maximum value $4U_{dc}/3\sqrt{(3)}$ which is the length of line OE, the actual output voltage trajectory jumps between vertices, i.e. point A, point B, ... , which is 6-step operation.

2.2.5 Discontinuous Modulation

The previous modulation strategies have established an equal distribution of the null vector or commonly known as the zero space vector in the space vector modulation technique. The zero space vector also serves as the fundamental building block for various PWM techniques. These strategies have the advantage of eliminating one switching transition in a half carrier cycle. Based on the above premise, different discontinuous PWM techniques have been established in literature [6]. The most commonly used methods are a namely 30-degree clamp, 60-degree clamp, and 120-degree clamp. In this work, only the 60-degree clamp is studied and analyzed, but a brief discussion on the implementation of the other techniques will be done in the implementation section.

2.2.5.1 DPMW1

This type of discontinuous modulation technique is also termed as the 60-degree clamp. The name briefly gives an idea of how the reference signal waveform would look like. The generation of zero sequence or common mode signal injected to the three-phase sinusoidal modulating signals is relatively simple, of the three-phase sinusoidal modulating signals the one that passes the maximum magnitude test at a given time interval is considered to be the common mode signal. Post addition of the zero sequence as mentioned earlier signal results in two 60 degrees clamped segments. Once in overmodulation, the resultant signal is upward shifted by an amount decided by the value of modulation index. The Fourier analysis of the saturated segment is determined in [9]. Figure 2.16 illustrates the 3 phase sinusoidal modulating signal, figure 2.17 and 2.18 exhibit the common mode post maximum magnitude test and the resultant waveform after common mode injection, respectively.

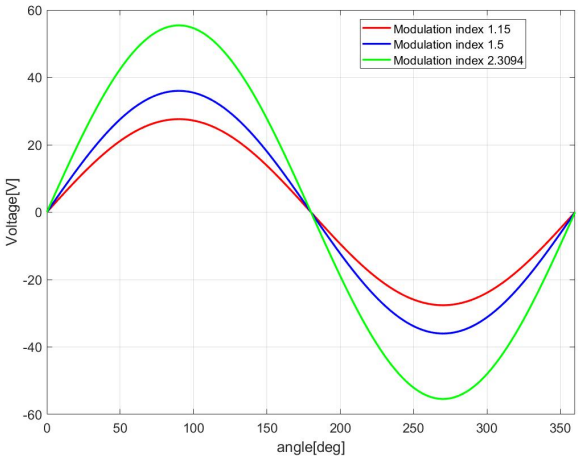

Figure 2.16: Variation of modulating waveform without common mode injection for DPWM1.

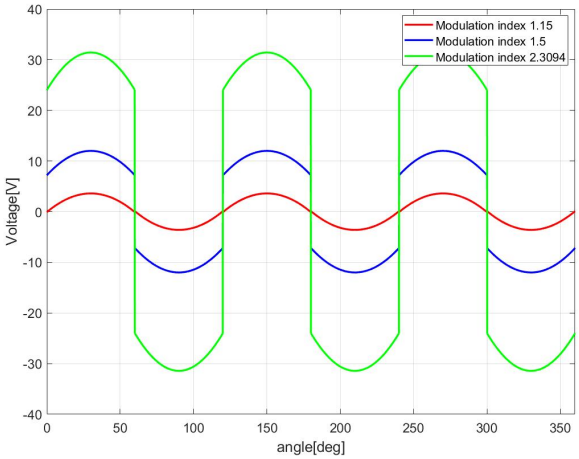

Figure 2.17: Variation of common mode injection for DPWM1.

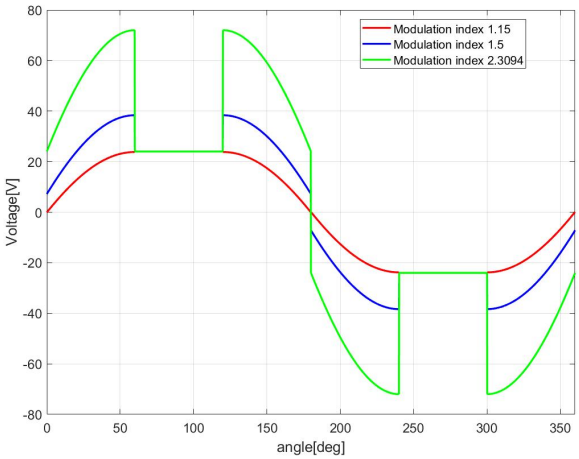

Figure 2.18: Variation of modulating waveform with increased overmodualtion for DPWM1.

2.2.5.2 DPMW0

In this type of discontinuous PWM, the common mode determination procedure is very similar to DPWM1. The 3 phase modulating reference signal waveforms are shifted 30 in phase and then passed through the maximum magnitude test, the signal which has the maximum value at a given instant decides the common mode or zero sequence signal. The complexity of this type of waveform is increased as it is no longer quarter wave symmetric. The details of the Fourier analysis can be found in [9]. The figure 2.19 and 2.20 exhibit the common mode and resultant waveform after addition of common mode for different modulation indices.

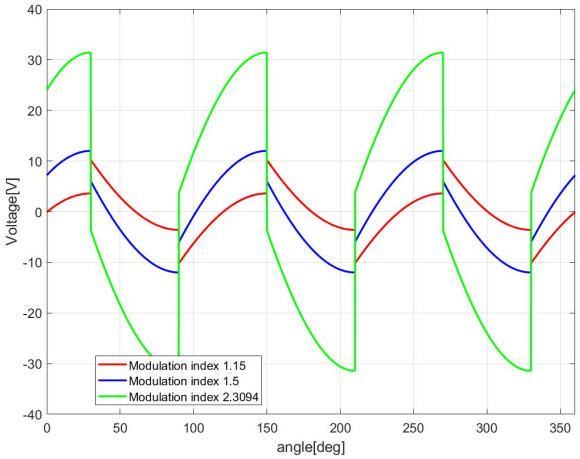

Figure 2.19: Variation of common mode injection for DPWM0.

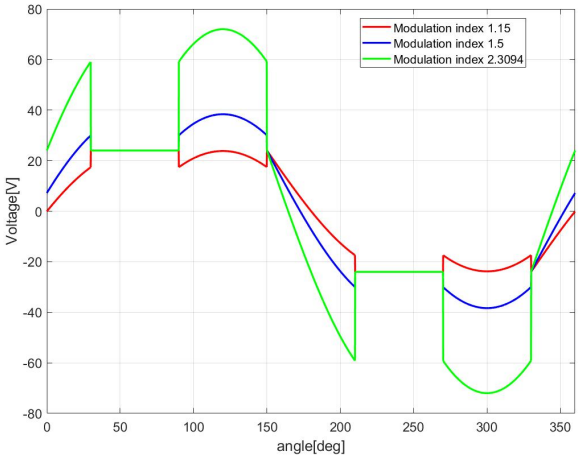

Figure 2.20: Variation of modulating waveform with increased overmodulation for DPWM0.

2.3 Performance evaluations

In this section, the motive of this thesis work is discussed. The aim is to evaluate the performance of different modulation techniques on an electric machine. The analysis is not limited to modulators, but also the loss consequence in the machine is analyzed i.e. copper loss and iron loss when the machine is subjected to different degrees of overmodulation. The parameters closely analyzed are the extra torque, machine losses, total harmonic distortion, inverter losses which include switching loss and conduction loss for a sic based mosfet inverter suited for a mild hybrid vehicle.

2.3.1 Extra Torque

It can be observed from figure 2.21, that with the increase in modulation index, there is an increase in the fundamental component of the output phase voltage fed to the machine. In the field weakening region of the torque-speed characteristics of an electric machine where the voltage constraint is active, the increase in fundamental voltage results in an increase in the average torque of the machine as is evident from fig 2.21, this, in turn, results in expanded power output from the machine. The fig 2.21 demonstrates the increase in power available from linear modulation range to 95% overmodulation. The expanded power range is maximized when the modulator is pushed to the maximum modulation limit, which is the 6 step operation where the maximum fundamental voltage is realized.

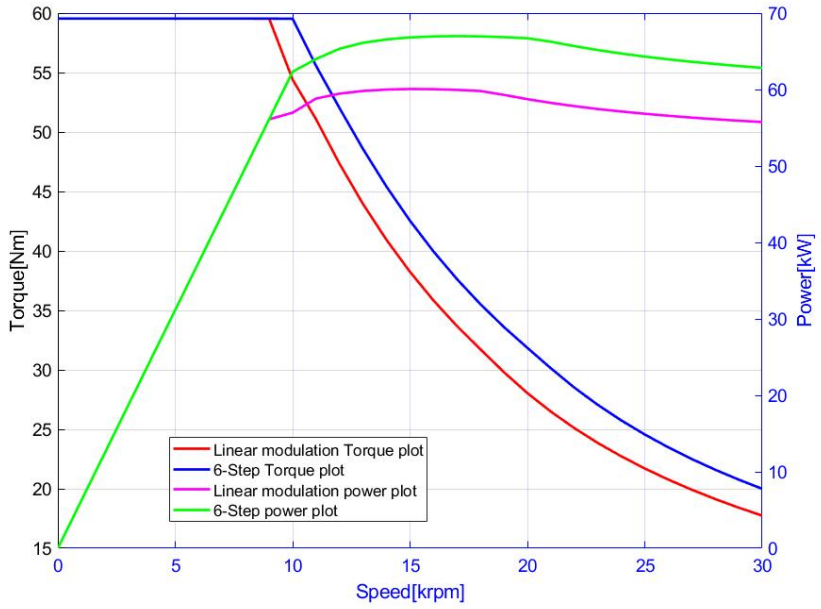

Figure 2.21: Power and Torque variation with speed in linear and overmodulation region.

2.3.2 Machine losses

The main loss components of an electric machine are joule losses and core losses. The joule losses are current magnitude and stator resistance dependant, and this loss component forms the major loss component in a 48V system because of higher current ratings. On the other hand, the iron loss is the result of changing flux densities in the various parts of the iron structure in the electric machine.

Core loss in the iron structure of an electric machine occurs when the core is subjected to time-varying magnetic flux densities. The nature of core loss can be classified into two different types of losses : eddy current loss and hysteresis loss. Hysteresis loss is the energy used up in redirecting magnetic domains of magnetic material during reversal of flux in the iron core. This type of loss is dependant on

material type and peak flux density[10]. Eddy current loss is due to the occurrence of circulating currents induced in the core material due to change in magnetic flux. This type of loss is dependant on the geometry of the material, harmonics in the air gap field flux and the rate of change of flux [10].

2.3.2.1 Analysis of Machine Losses

There have been several methods reported to evaluate core losses for an electric machine in literatures, for example in [10]. Some of the methods include : Empirical formula method, FEM , Search coil method. In the empirical method the waveform of the flux density at the teeth is approximated as a trapezoid. The eddy current loss in the tooth is estimated as

$$P_{eddy(T)} = \frac{pr}{\pi^2 l_T} k_e w_n^2 B_T^2 \tag{2.37}$$

where p is the number of pole pairs, r is the radius of air gap, l_T is the width of the teeth that the magnet traverses, k_e is the eddy current loss constant, w_n is the mechanical speed of the machine in rpm, B_T is the maximum flux density in the tooth. Similarly, the eddy current loss in the back iron is estimated as

$$P_{eddy(Y)} = \frac{2p}{\pi^3 \alpha_m} k_e w_n^2 B_Y^2 \tag{2.38}$$

Where α_m is the pole arc, B_Y is the maximum flux density in the back iron. The summation of the two components of the eddy current loss results in the eddy current loss in the stator, with the knowledge of the volume of iron used and mass density of the material the 2.24 and 2.25 can be re-written as

$$P_{eddy(stator)} = \frac{p k_e w_n^2 \delta}{\pi^3} (V_T \frac{r}{l_T} B_T^2 + V_Y \frac{2}{\alpha_m} B_Y^2) \tag{2.39}$$

where V_T and V_Y are the volume of material used in teeth and back iron of the stator. δ is the mass density of the material used which readily available from material datasheet. The hysteresis loss can be evaluated in a similar way,

$$P_{hys} = \frac{p k_h w_n \delta}{2\pi} (V_T B_T^n + V_Y B_Y^n) \tag{2.40}$$

The details on the derivation of the equations demonstrated in this section and the other methods for determination of core loss can be found in [10]. It is to be noted that this method is valid when the electric machine is fed with a sinusoidal voltage source, which is not the case for inverter-fed electric machines. Therefore to be able to analyze or estimate core losses due to switched waveform or PWM, a different method is adopted.

2.3.2.2 Analysis of Core loss due to PWM

This approach is also known as Fast Method for Iron Loss prediction in Inverter-Fed Induction Motors [11]. The eddy current and hysteresis loss can be represented as

$$P_{eddy} = K_e f B_p^x \tag{2.41}$$

$$P_{hysteresis} = K_h f^2 B_p^2 \tag{2.42}$$

where K_e, K_h , f, B_p are the eddy current loss constant, hysteresis loss constant, frequency of operation, B_p is the peak flux density in the area of interest. According to [11] if the iron losses of the machine and the two-loss contributions are known then a variation is to be expected due to voltage waveform source. Since the peak flux density is of prime importance, it can be estimated with respect to voltage as

$$B_p = \frac{V_{av}}{4NS}T = k\frac{V_{av}}{f} \tag{2.43}$$

where V_{av} is the average rectified value of the alternate voltage waveform, N is the number of turns and S is the area of interest. From the peak flux density the hysteresis loss can now be re-written as

$$P_{hys} = \zeta V_{av}^x f^{1-x} \tag{2.44}$$

where ζ is material coefficient. Similarly the eddy current loss equation as a function of the rms voltage can be represented as

$$P_{eddy} = 2\sigma V_{rms}^2 \tag{2.45}$$

where σ is a material coefficient and V_{rms} is the supple voltage rms value. Now that the equations of core loss as a function of average and rms value have been identified a new set of equation can be developed for core loss due to switched voltage waveform.

$$P_{stator} = \eta^x P_{h,sine} + \beta^2 P_{e,sine} \tag{2.46}$$

where $P_{h,sine}$ and $P_{e,sine}$ are the hysteresis and eddy current loss due to sinusoidal supply. η and β are defined as follows

$$\eta = \frac{V_{av}}{V_{av,fund}} \tag{2.47}$$

$$\beta = \frac{V_{rms}}{V_{rms,fund}} \tag{2.48}$$

V_{av} is the voltage mean rectified value, $V_{av,fund}$ is the mean rectified value of the fundamental voltage, V_{rms} is the rms of the voltage source, $V_{rms,fund}$ is the rms value of the fundamental voltage. The details of the derivation of all equations described in this section can be found in [11]. It has been observed that for very high ratios between fundamental and carrier frequency, the term η is unity implying that hysteresis loss is almost constant and thereby the significant contribution is from the eddy current loss[ref].

2.3.3 THD

The total harmonic distortion (THD) is a measurement of the harmonic distortion present in a signal and is defined as the ratio of the sum of the powers of all harmonic components to the power of the fundamental frequency. THD could be analysied by fast fourier transform (FFT) based on

$$THD = \frac{\sqrt{h_1^2 + h_2^2 + h_3^2 + ... + h_n^2}}{f_1} \tag{2.49}$$

where h_1 is first harmonic component and f_1 is fundemental component. FFT-based THD analysis could be conducted by using the above equation or Matlab Powgui toolbox automatically.

2.3.4 Semiconductor losses

Conduction and switching losses are considered in this case while blocking(leakage) losses are neglected. A calculation for semiconductor power losses based on datasheet parameters in a three-phase Ac motor drive applications are as follows [12]. The topology is shown in Fig. 2.22

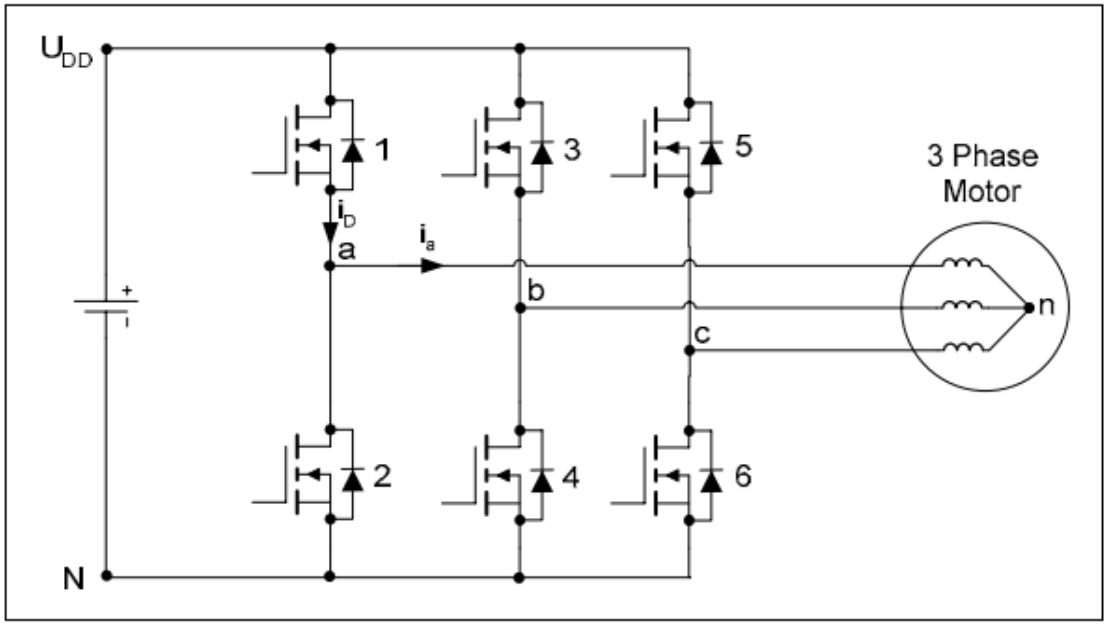

Figure 2.22: Three-phase AC motor drive.

2.3.4.1 Conduction losses

The conduction losses occur when the MOSFET or diode is conducting. An instantaneous method performed by detecting switching actions is used for the conduction losses calculation. The instantaneous value of MOSFET conduction losses can be written as

$$p_{CM}(t) = u_{DS}(t)i_D(t) = R_{DSon}i_D^2(t) \tag{2.50}$$

and the average MOSFET power loss over one switching period is

$$P_{CM} = R_{DSon}{I_{Drm}}_s^2 \tag{2.51}$$

where u_{DS} is drain-source voltage, i_D is drain current, I_{Drms} is the rms value of drain current over one switching period, R_{DSon} is drain-source on-state resistance

which could be read from the data-sheet diagram. The instantaneous value of the diode conduction losses can be similarly written as

$$p_{CD}(t) = u_D(t)i_F(t) = u_{D0}(t)i_F(t) + R_D i_F^2(t) \tag{2.52}$$

and the average diode power loss over one switching period is

$$P_{CD} = u_{D0}I_{Favg} + R_D {I_{Frms}}^2_s \tag{2.53}$$

where u_D is the voltage across the diode, i_F is the current through the diode, I_{Drms} is the average value of the current through the diode over one switching period, I_{Drms} is the rms value of the current through the diode over one switching period, u_{D0} and R_D are diode on-state zero current voltage and diode on-state resistance which could be read from the data-sheet diagram. While a switching action is detected, the current at that moment is recorded and other parameters in the equation are from a data-sheet as stated.

2.3.4.2 Switching losses

The switching losses occur when the MOSFET or diode is in the process of turning on or turning off. Switching losses are the product of switching energies and switching frequency which could be written as

$$P_{swM} = (E_{onM} + E_{offM})f_{sw} \tag{2.54}$$

$$P_{swD} = (E_{onD} + E_{offD})f_{sw} \approx E_{offD}f_{sw} \tag{2.55}$$

since the switch on losses in the diode are normally neglected, where f_{Sw} is switching frequency, E_{onM}, E_{offM}, E_{onD}, E_{offD} are MOSFET switching on energy, MOSFET switching off energy, diode switching on energy, diode switching off energy which could be calculated from data-sheet, the calculations can be found in [12]. For discontinuous PWM, the above equation is not valid anymore since the switching losses become dependent on phase angle, switching loss function(SLF) is needed to normalize different modes of discontinuous PWM to continuous PWM. The switching loss function is defined as

$$SLF = \frac{P_{swDPWM}}{P_{sw}} \tag{2.56}$$

where P_{swDPWM} is switching losses of DPWM and P_{sw} is the switching losses for continousPWM. A general equation for calculating SLF is given by

$$SLF = \begin{cases} \frac{\sqrt{(3)}}{2}cos(\frac{4\pi}{3} + \beta - \theta_s) & -\frac{\pi}{2} < \theta_s < -\frac{\pi}{2} + \beta \\ 1 - \frac{1}{2}cos(\frac{\pi}{3} + \beta - \theta_s) & -\frac{\pi}{2} + \beta < \theta_s < \frac{\pi}{6} + \beta \\ \frac{\sqrt{(3)}}{2}cos(\frac{\pi}{3} + \beta - \theta_s) & \frac{\pi}{6} + \beta < \theta_s < \frac{\pi}{2} \end{cases} \tag{2.57}$$

where θ_s is the angle between phase current and voltage, which is measured by detecting zero-crossing of voltage and phase current in Matlab then calculating the phase difference. β is the modulator phase angle increasing from the intersection

point of two reference modulation waves. The β angle for DPWM0, DPWM1, DPWM2 are 0, $\frac{\pi}{6}$, $\frac{\pi}{3}$ respectively. The switching loss function of DPWMMAX and DPWMMIN is given by

$$SLF_{DPWMMAX} = \begin{cases} \frac{1}{2} - \frac{1}{4}sin\theta_s & -\frac{\pi}{2} < \theta_s < -\frac{\pi}{6} \\ 1 - \frac{\sqrt{3}}{4}cos\theta_s & -\frac{\pi}{6} < \theta_s < \frac{\pi}{6} \\ \frac{1}{2} + \frac{1}{4}sin\theta_s & \frac{\pi}{6} < \theta_s < \frac{\pi}{2} \end{cases} \tag{2.58}$$

$$SLF_{DPWMMAX} = SLF_{DPWMMIN} \tag{2.59}$$

3
Implementation and waveforms

3.1 MATLAB modelling

The work presented in this thesis is to determine the extra power, and the loss consequences from an SP-IPMSM modeled in 2D finite element environment. The procedure is to generate the switched voltage waveform from the modulators for different modulation techniques in the over-modulation region, then utilizing these switched waveform a voltage excited simulation is carried out in Ansys Maxwell. The procedure of implementation is explained in this section. The fig 3.1 illustrates an open loop mathematical model built to generate switched waveforms.

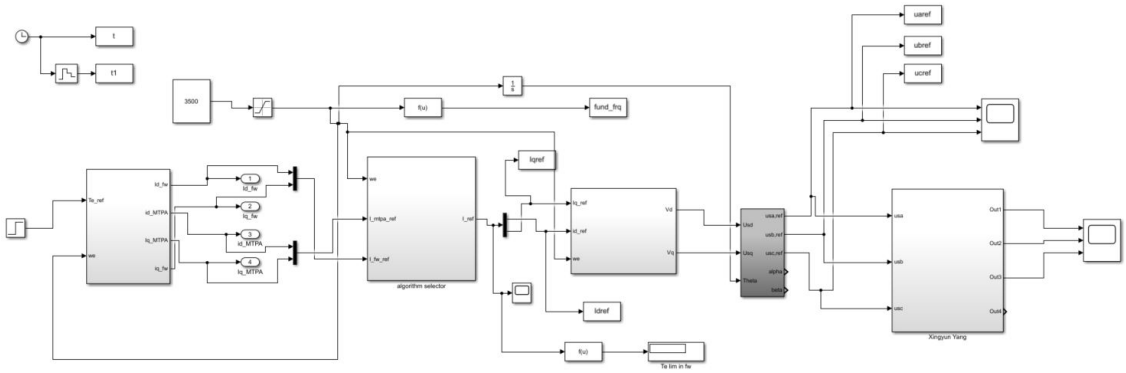

Figure 3.1: MATLAB model to generate switched waveform for different modulation techniques.

3.1.1 Reference current generation

In this section, the reference current generation strategy is discussed. As already explained in section 2.1.4, there are two regions in the torque-speed characteristics known as constant torque region and constant power region. The regions can also be distinguished by the type of current or voltage constraint that limits the operation in that particular region. The strategy used in the constant torque region is called MTPA, and the control in the constant power region is called the field weakening strategy. The point of interest in this work is to investigate steady-state operating points. Therefore, a steady state control method is used to find the appropriate current references during operation.The control method is highly influenced by the saturation of L_{sd},L_{sq} and variations in Ψ_m which are functions of I_{sd} and I_{sq} respectively [5]. The MTPA strategy is obtained by finding a solution to the following

minimization problem with an equality constraint $h(i_{sd}, i_{sq})$ [5].

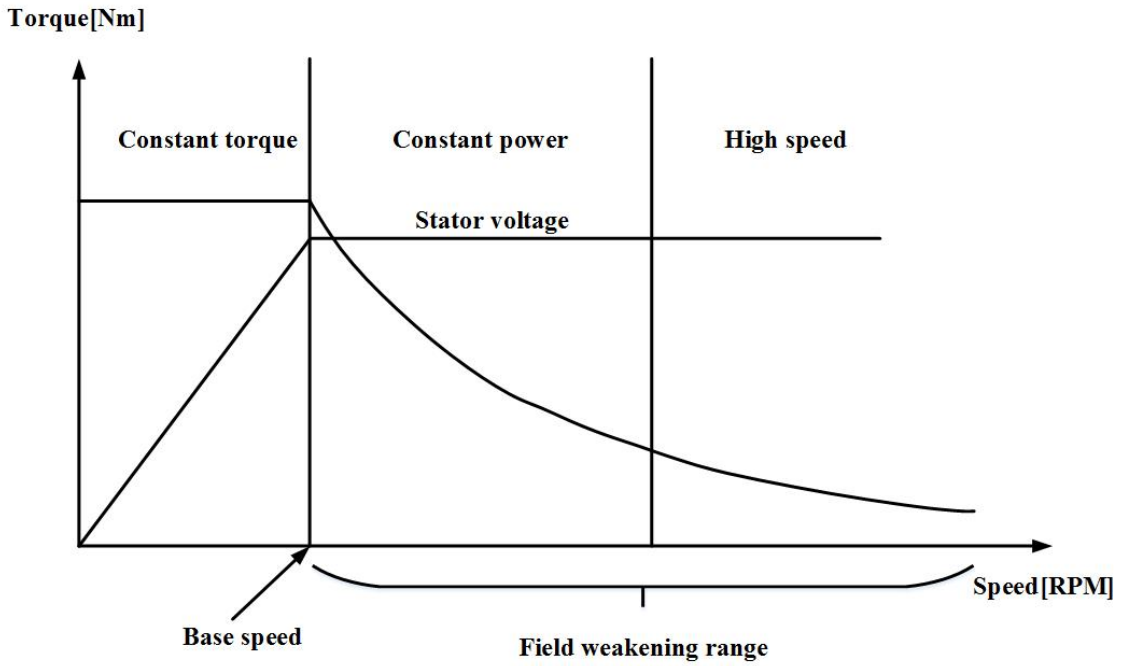

Figure 3.2: Torque-speed characteristics of IPMSM .

$$minimize f(I_{sd}, I_{sq}) = \sqrt{(i_{sd}^2 + i_{sq}^2)} \tag{3.1}$$

$$h(i_{sd}, i_{sq}) = 1.5 n_p i_{sq}[\Psi_m + (i_{sq}) + L_{sd}(i_{sd}, i_{sq}) - L_{sq}(i_{sd}, i_{sq}) i_{sd}] - T_{e,ref} = 0 \tag{3.2}$$

Whereas in the field weakening region the constraints are described by maximizing the available torque with an equality and non equality constraint in the form of $h(i_{sd}, i_{sq})$ and $j(i_{sd}, i_{sq})$ respectively [5].

$$maximize f(i_{sd}, i_{sq}) = 1.5 n_p i_{sq}[\Psi_m + (i_{sq}) + L_{sd}(i_{sd}, i_{sq}) - L_{sq}(i_{sd}, i_{sq}) i_{sd}] \tag{3.3}$$

$$h(i_{sd}, i_{sq}) = \sqrt{(U_{sd}(i_{sd}, i_{sq})^2 + U_{sq}(i_{sd}, i_{sq})^2) - U_{max}^2} = 0 \tag{3.4}$$

$$j(i_{sd}, i_{sq}) = \sqrt{(i_{sd}^2 + i_{sq}^2) - I_{max}^2} <= 0 \tag{3.5}$$

The current references in the form of i_{sd} and i_{sq} obtained are used further in the model to generate u_{sd} and u_{sq}.

3.1.2 Reference voltage generation

The requirement for any modulation technique implemented using space vector method requires voltages in the stationary reference frame i.e $u_{s\alpha}$ and $u_{s\beta}$. This

transformation is possible using park transformation, which utilizes rotor angle to move from a synchronously rotating frame to stationary rotating frame. The d and q axis equivalent circuit models are used to determine the u_{sd} and u_{sq} using equations

$$u_{sd} = R_s i_{sd} - \omega_r L_{sq} i_{sq} \tag{3.6}$$

$$u_{sq} = R_s i_{sq} + \omega_r L_{sd} i_{sd} + \omega_r \Psi_m \tag{3.7}$$

3.1.3 Modulator

3.1.3.1 Classical Overmodulation Implementation

This section describes the implementation of SPWM in MATLAB. As evident from the fig 3.4 three sinusoidal signals with a phase shift of 120° is used to generate the modulating signal i.e. the voltage magnitude of the reference voltage is normalized to the modulation index. Considering the definition of modulation index used, the carrier signal is normalized to the value of modulation index in linear modulation region, therefore, any signal value over the prescribed value of 1.15 would result in overmodulation.

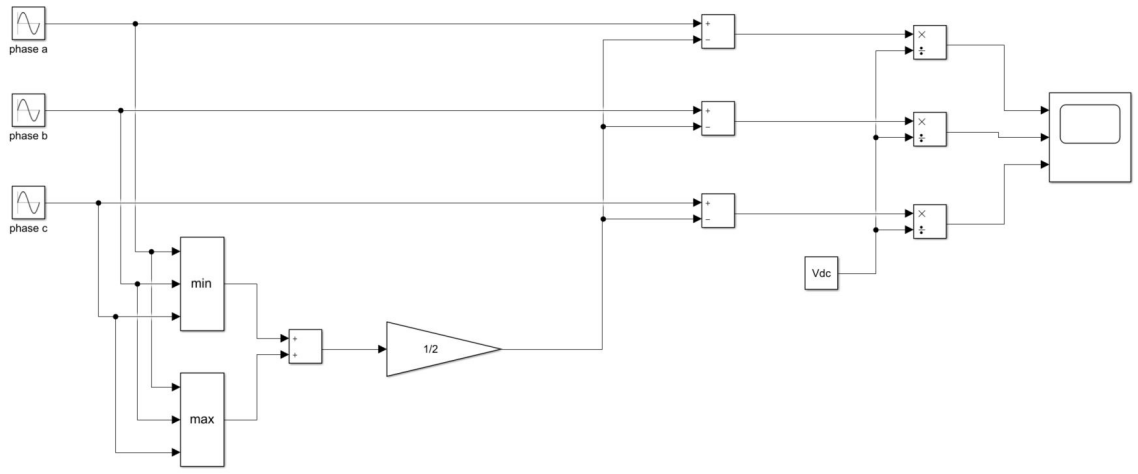

Figure 3.3: Classical Over-modulation with zero sequence injection implementation in MATLAB .

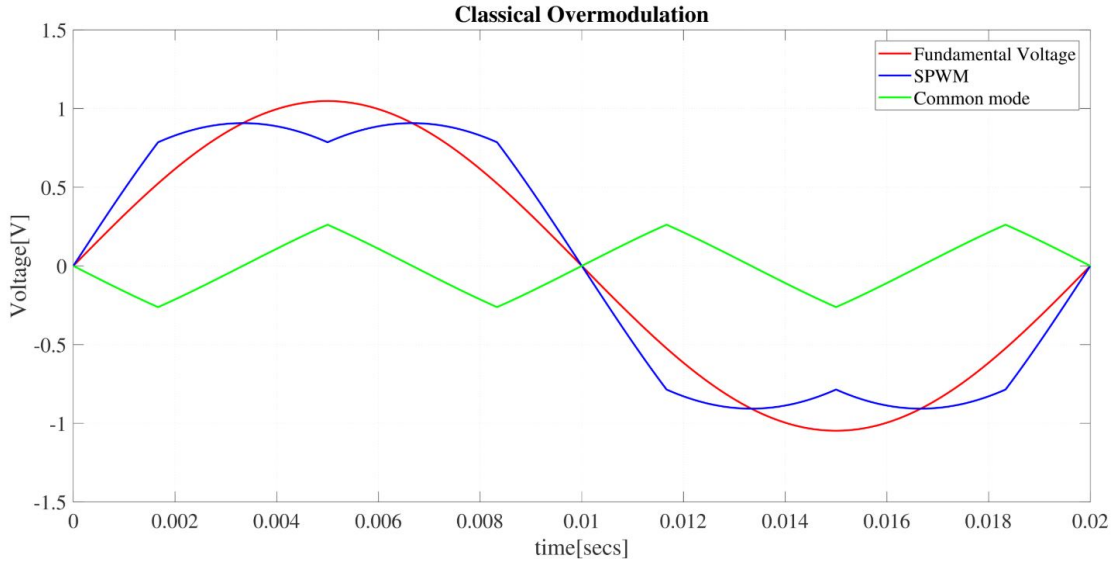

Figure 3.4: Classical Over-modulation with zero sequence injection implementation in MATLAB .

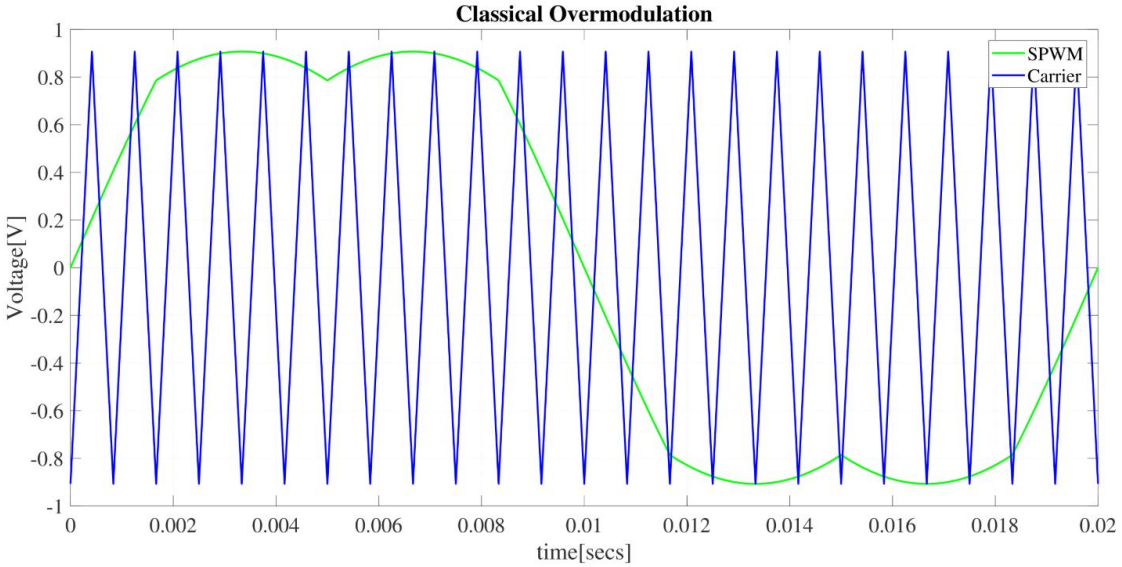

Figure 3.5: Classical Over-modulation waveform with triangle comparison .

3.1.3.2 SVM

For any given space voltage vector U_{ref}, the α and β axis component U_α and U_β can be determined. Therefore three decision variables A, B and C are defined which have the following relationship with U_α and U_β[13]:

$$\begin{cases} U_\beta > 0, & A = 1 \quad else \quad A = 0 \\ \sqrt{3}U_\alpha - U_\beta > 0, & B = 1 \quad else \quad B = 0 \\ -\sqrt{3}U_\alpha - U_\beta > 0, & C = 1 \quad else \quad C = 0 \end{cases} \tag{3.8}$$

An intermediate variable N is defined as

$$N = A + 2B + 4C \tag{3.9}$$

which has the following relationship with sector number shown in Table.3.1.

Table 3.1: Relation between value of N and sector number.

sector	I	II	III	IV	V	VI
N	3	1	5	4	6	2

An example of N number changing during 10 switching period is shown in Fig.3.6.

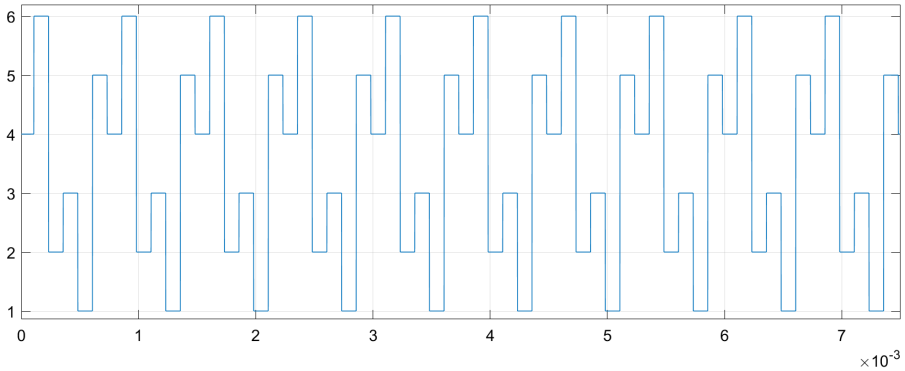

Figure 3.6: Changing of N during 10 switcing period.

The next step is to determine the time applied on different basic voltage vector. Define the time applied on any two active voltage vectors as T_1 and T_2, during one switching period, the time applied on the zero voltage vector U_0 and U_7 as T_0 and T_7. Take sector I as an example, according to voltage-second balance, one would have the following equation

$$\begin{cases} U_\alpha T = |U_4|T_1 + \frac{1}{2}|U_6|T_2 \\ U_\beta T = \frac{\sqrt{3}}{2}|U_6|T_2 \end{cases} \tag{3.10}$$

where T is the switching period, T_1 is the time applied on voltage vector U_4, T_2 is the time applied on voltage vector U_6 during one switching period, $|U_4|$ and $|U_6|$ equals to $2/3U_d$.

Therefore the time T_1 and T_2 could be solved from (3.13)

$$\begin{cases} T_1 = \frac{\sqrt{3}T}{2U_d}(\sqrt{3}U_\alpha - U_\beta) \\ T_2 = \frac{\sqrt{3}U_\beta T}{U_d} \\ T_{0,7} = T - T_1 - T_2 \end{cases} \tag{3.11}$$

In order for convenient calculation, define three intermediate variables X, Y, Z as

$$\begin{cases} X = \sqrt{3}\frac{T}{U_d}U_\beta \\ Y = \frac{T}{U_d}(\frac{\sqrt{3}}{2}U_\beta + \frac{3}{2}U_\alpha) \\ Z = \frac{T}{U_d}(\frac{\sqrt{3}}{2}U_\beta - \frac{3}{2}U_\alpha) \end{cases} \tag{3.12}$$

The sector's relationship with T_1 and T_2 are shown in Table 3.2. For overmodulation where $T_1 + T_2 > T$, then T_1 and T_2 could be linearized as

$$\begin{cases} T_1 = \frac{T_1}{T_1+T_2}T \\ T_2 = \frac{T_2}{T_1+T_2}T \end{cases} \tag{3.13}$$

Table 3.2: Relation between Switching time and sector number.

Time/Sector	I	II	III	IV	V	VI
T_1	Z	Y	-Z	-X	X	-Y
T_2	Y	-X	X	Z	-Y	-Z

Therefore T_1 and T_2 can be calculated from X, Y, Z and T.

After getting the applied time T_1 and T_2 on two basic voltage vectors, the output voltage vector in different sectors corresponding to each phase bridge arm switch time point can be derived, time signal T_{cm1}, T_{cm2}, T_{cm3} for phase A, B, and C has following relation with T_1, T_2 and the sector as shown in Table 3.3.

Table 3.3: Sector and Switch conduction time

phase/sector	I	II	III	IV	V	VI
A	Tcm2	Tcm1	Tcm1	Tcm3	Tcm3	Tcm2
B	Tcm1	Tcm3	Tcm2	Tcm2	Tcm1	Tcm3
C	Tcm3	Tcm2	Tcm3	Tcm1	Tcm2	Tcm1

In the table, T_{cm1}, T_{cm2}, T_{cm3} is defined as

$$\begin{cases} Tcm1 = \frac{T-T1-T2}{2} \\ Tcm2 = \frac{T+T1-T2}{2} \\ Tcm3 = \frac{T+T1+T2}{2} \end{cases} \tag{3.14}$$

Therefore, the switching pattern could be generated by comparing the time signal T_{cm1}, T_{cm2}, T_{cm3} and the triangular wave as shown in Fig. 3.7.

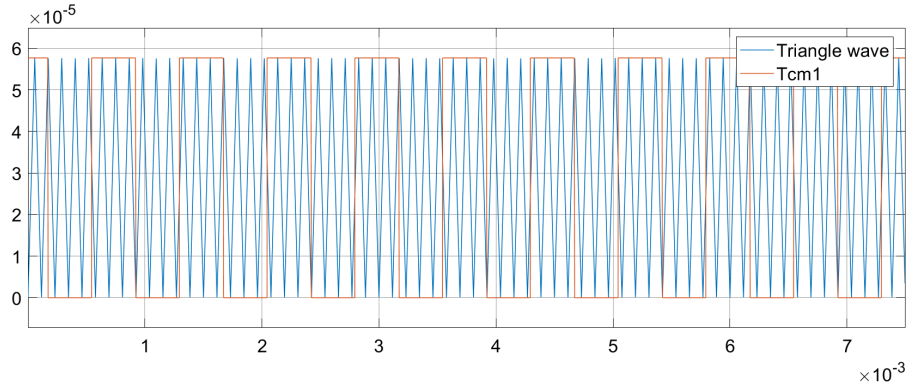

Figure 3.7: Switching pattern generation by comparing the time signal and the triangular wave for phase A.

A complete implementation for space vector modulation including the inverter model in MATLAB is described in Fig.3.8.

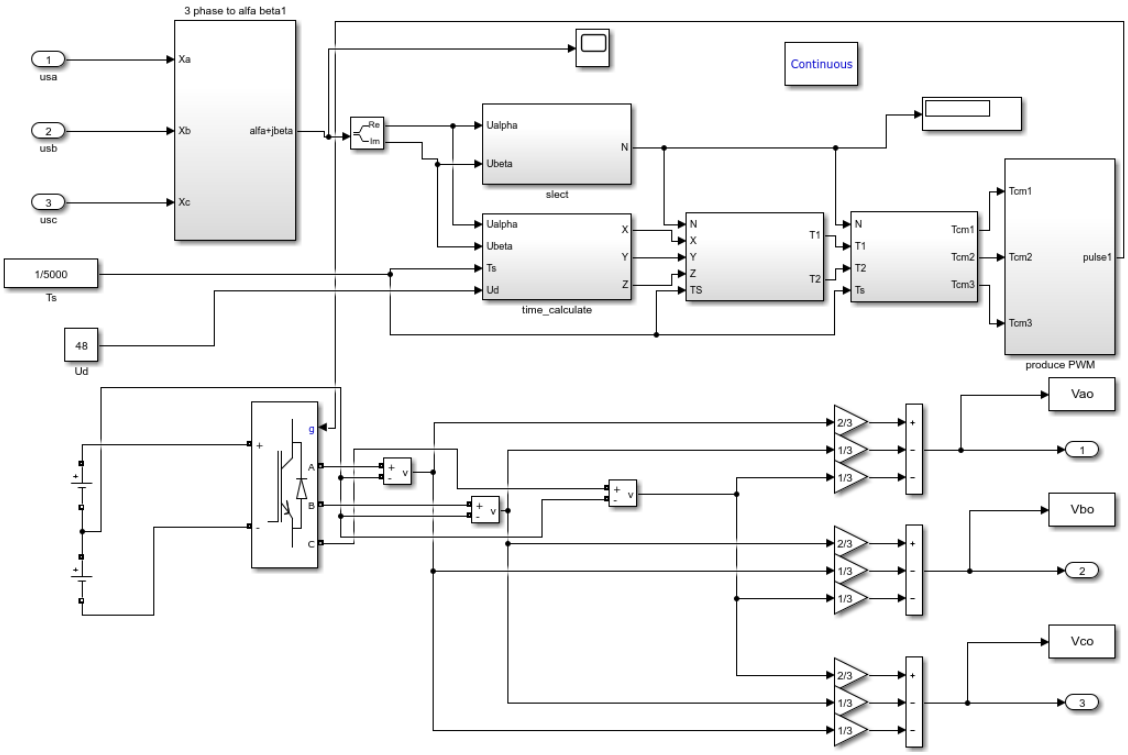

Figure 3.8: Space vector modulation implementation in MATLAB.

3.1.3.3 DPWM1

It has been discussed in chapter 2 that the way to generate the reference signal for DPWM techniques is first to determine the common mode signal. To be able to use a generalized approach to develop the PWM techniques a high-performance generalized DPWM technique is utilized [9]. An operator ψ is introduced, which will be utilized to move between different dpwm techniques [9]. The operator is termed as modulator phase angle. As reported in [9], ψ increases from the intersection of the two reference signal at $w_e t = \pi/6$. This aids in determining the modulating signal, the signal that passes the maximum magnitude test(MMT) comprises the common mode signal. When evaluating the maximum magnitude test, three sinusoidal reference signals are phase shifted by $\psi - \pi/6$ and three new signals are obtained, the maximum magnitude at a given time decides the common mode signal. For instance, if 3 sinusoidal phase signals are defined as V_a^*,V_b^*,V_c^* shown in figure 3.9. Then they are phase shifted using $\psi - \pi/6$, for dpwm1 the value of the phase modulator is taken to be $\pi/6$, implying that the signals remain unchanged, they are renamed as V_{ax}^*,V_{bx}^*,V_{cx}^*.

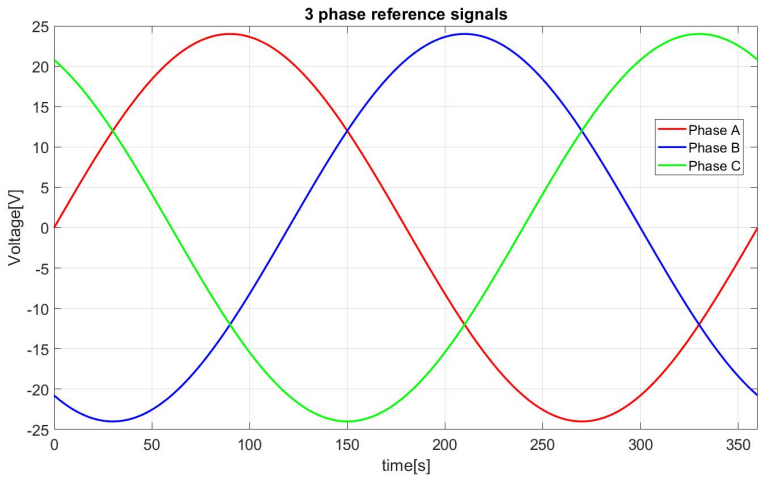

Figure 3.9: Three phase reference signal.

The next step is to impose the following criteria of the MMT,

$$if \quad |V_{ax}^*| >= |V_{bx}^*|$$

$$and \quad |V_{ax}^*| >= |V_{cx}^*|$$

$$V_{ax}^{**} = sign(V_{ax}^*)\frac{V_{dc}}{2} - V_{ax}^*$$

$$if \quad |V_{bx}^*| >= |V_{ax}^*|$$

$$and \quad |V_{bx}^*| >= |V_{cx}^*|$$

$$V_{bx}^{**} = sign(V_{bx}^*)\frac{V_{dc}}{2} - V_{bx}^*$$

$$if \quad |V_{cx}^*| >= |V_{ax}^*|$$
$$and \quad |V_{cx}^*| >= |V_{bx}^*|$$
$$V_{cx}^{**} = sign(V_{cx}^*)\frac{V_{dc}}{2} - V_{cx}^*$$

Combining V_{ax}^{**},V_{bx}^{**},V_{cx}^{**} the common mode signal or zero sequence is represented as

$$V_{cm} = V_{ax}^{**} + V_{bx}^{**} + V_{cx}^{**}$$

Post the implementation of the MMT as mentioned earlier algorithm the common mode obtained is shown in figure 3.10. This resultant common mode added to the 3 phase reference signal results in the modified dpwm 60 degrees clamped waveform as shown in figure 3.11

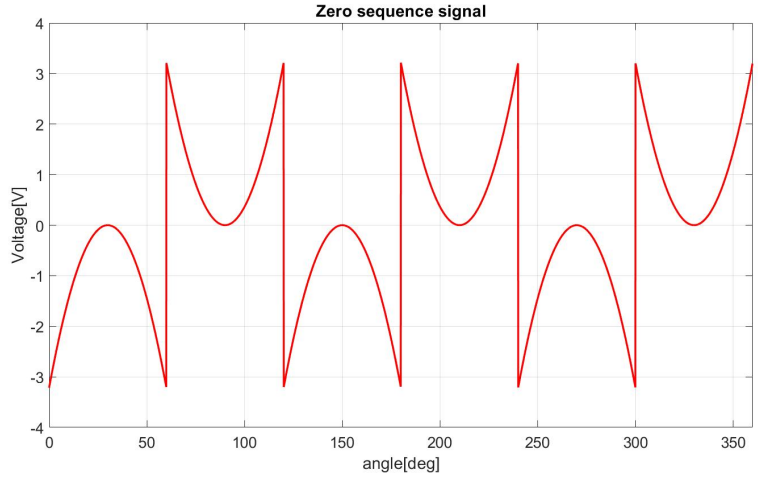

Figure 3.10: Zero sequence signal.

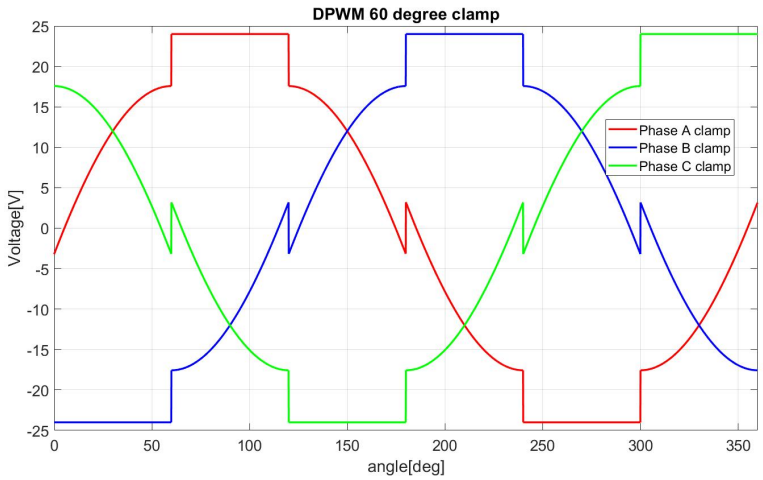

Figure 3.11: DPWM 60 degree clamp signals.

3.1.3.4 DPWM2

This is also known as dpwm 60-degree leading clamp. In this case, the reference 3 phase signals are phase shifted by the modulator phase operator. For dpwm2 the value for ψ is $pi/6$. Similar to the case of dpwm1, the MMT is applied to dpwm2 the only difference being the conditions imposed to evaluate the zero sequence signal.

$$if \quad |V_{ax}^*| >= |V_{bx}^*|$$

$$and \quad |V_{cx}^*| >= |V_{bx}^*|$$

$$V_{ax}^{**} = sign(V_{ax}^*)\frac{V_{dc}}{2} - V_{ax}^*$$

$$if \quad |V_{bx}^*| >= |V_{cx}^*|$$

$$and \quad |V_{ax}^*| >= |V_{cx}^*|$$

$$V_{bx}^{**} = sign(V_{bx}^*)\frac{V_{dc}}{2} - V_{bx}^*$$

$$if \quad |V_{cx}^*| >= |V_{ax}^*|$$

$$and \quad |V_{bx}^*| >= |V_{ax}^*|$$

$$V_{cx}^{**} = sign(V_{cx}^*)\frac{V_{dc}}{2} - V_{cx}^*$$

Post evaulation of MMT the common mode and clamped signals are presented in figure 3.12 and 3.13.

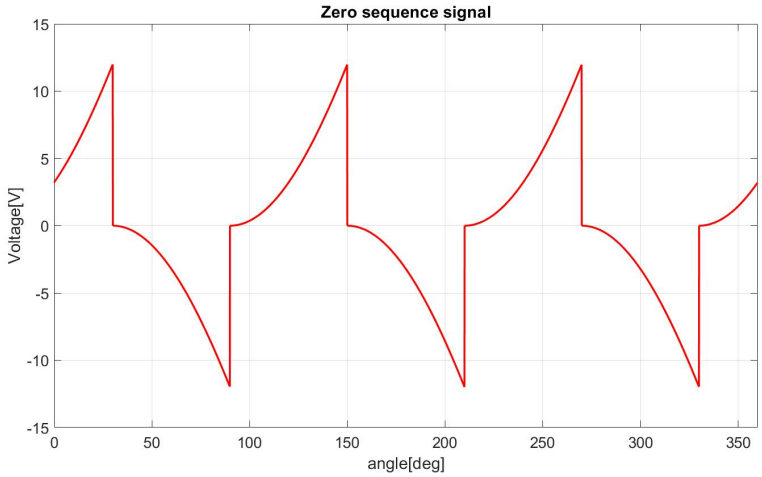

Figure 3.12: Zero sequence signal.

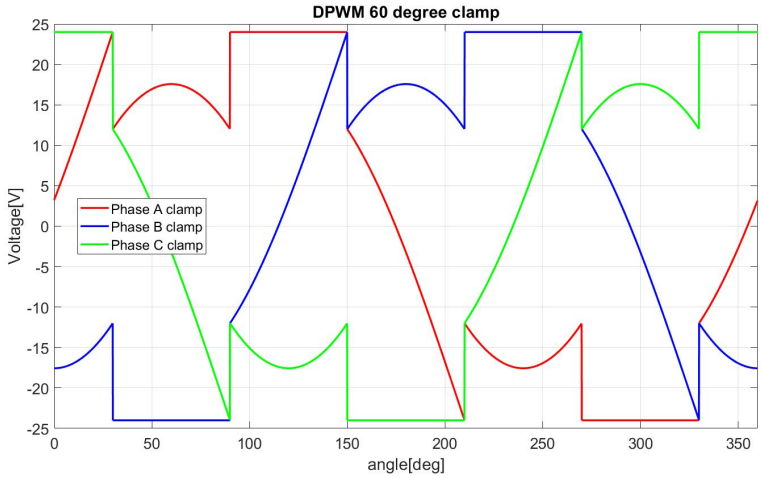

Figure 3.13: DPWM 60 degree leading clamp signals.

3.1.3.5 DPWM0

This technique is also known as dpwm 60 degree lagging clamp. The conditions for this technique to facilitate determination of common mode are

$$if \quad |V_{ax}^*| >= |V_{cx}^*|$$

$$and \quad |V_{bx}^*| >= |V_{cx}^*|$$

$$V_{ax}^{**} = sign(V_{ax}^*)\frac{V_{dc}}{2} - V_{ax}^*$$

$$if \quad |V_{cx}^*| >= |V_{bx}^*|$$

$$and \quad |V_{ax}^*| >= |V_{bx}^*|$$

$$V_{bx}^{**} = sign(V_{bx}^*)\frac{V_{dc}}{2} - V_{bx}^*$$

$$if \quad |V_{bx}^*| >= |V_{ax}^*|$$

$$and \quad |V_{cx}^*| >= |V_{ax}^*|$$

$$V_{cx}^{**} = sign(V_{cx}^*)\frac{V_{dc}}{2} - V_{cx}^*$$

Once the evaluaiton of MMT is done the zero sequence and clamped signals are presented as figure 3.14 and 3.15 respectively.

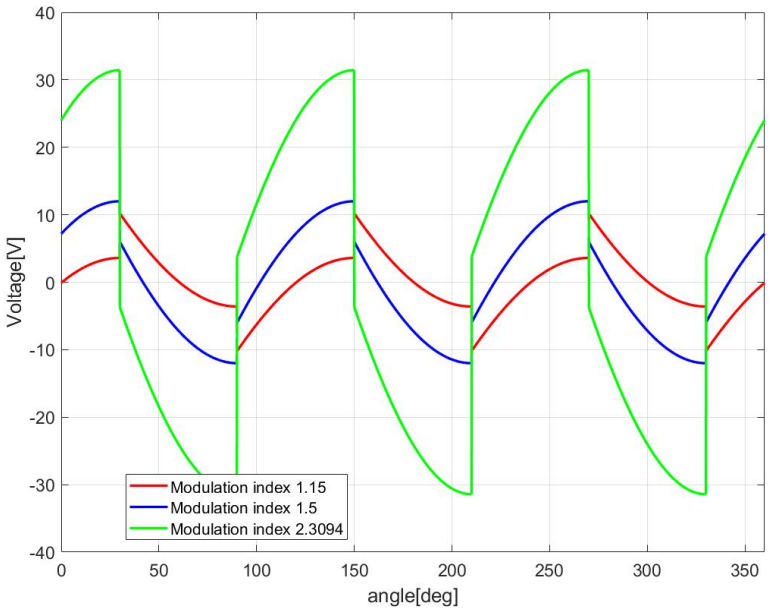

Figure 3.14: Zero sequence signal.

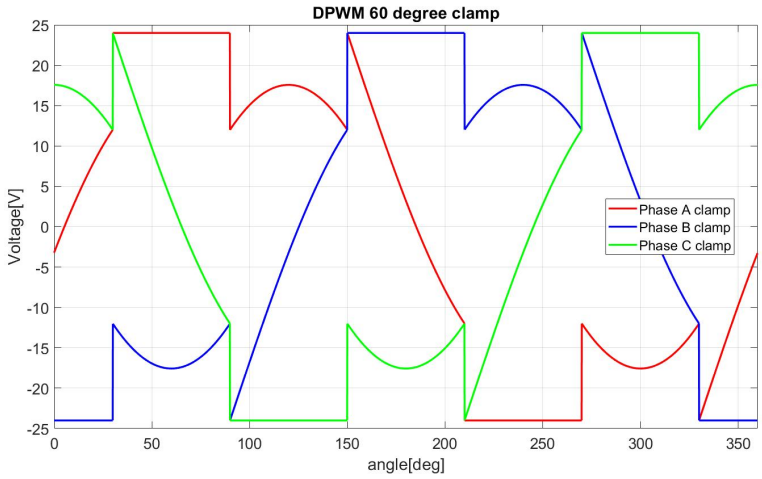

Figure 3.15: DPWM 60 degree lagging clamp signals.

3.1.3.6 DPWM3

This technique results in 30-degree clamping. The common mode determination is based on the fact that the intermediate signal among the three-phase reference signal decides the zeros sequence signal. The conditions are determined as

$$if \quad |V_{bx}^*| >= |V_{ax}^*| >= |V_{cx}^*|$$

$$V_{ax}^{**} = sign(V_{ax}^*)\frac{V_{dc}}{2} - V_{ax}^*$$

$$if \quad |V_{ax}^*| >= |V_{bx}^*| >= |V_{cx}^*|$$

$$V_{bx}^{**} = sign(V_{bx}^{*})\frac{V_{dc}}{2} - V_{bx}^{*}$$

$$if \quad |V_{bx}^{*}| >= |V_{cx}^{*}| >= |V_{ax}^{*}|$$
$$V_{cx}^{**} = sign(V_{cx}^{*})\frac{V_{dc}}{2} - V_{cx}^{*}$$

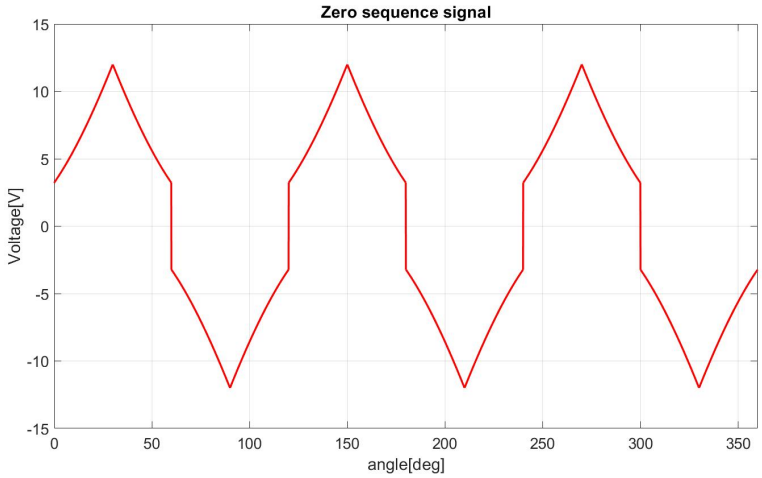

Figure 3.16: Zero sequence signal.

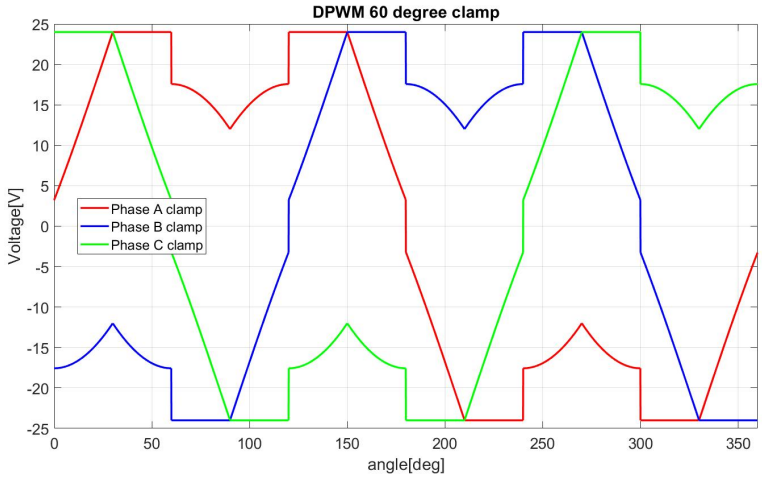

Figure 3.17: DPWM 30 degree clamp signals.

3.1.3.7 DPWM-MAX

This type of technique has its name based on the degree of clamping just like the others. The difference, in this case, is that it clamps one leg for 120 degrees. The determination of zero sequences is demonstrated as follows. It is to be noted that the phase modulator operator is no longer needed for 120-degree clamping methods.

$$if \quad |V_{ax}^{*}| >= |V_{bx}^{*}|$$

$$and \quad |V_{ax}^*| >= |V_{cx}^*|$$

$$V_{ax}^{**} = sign(V_{ax}^*)\frac{V_{dc}}{2} - V_{ax}^*$$

$$if \quad |V_{bx}^*| >= |V_{ax}^*|$$

$$and \quad |V_{bx}^*| >= |V_{cx}^*|$$

$$V_{bx}^{**} = sign(V_{bx}^*)\frac{V_{dc}}{2} - V_{bx}^*$$

$$if \quad |V_{cx}^*| >= |V_{ax}^*|$$

$$and \quad |V_{cx}^*| >= |V_{bx}^*|$$

$$V_{cx}^{**} = sign(V_{cx}^*)\frac{V_{dc}}{2} - V_{cx}^*$$

The common mode and clamped signals are presented in figure 3.18 and 3.21 respectively.

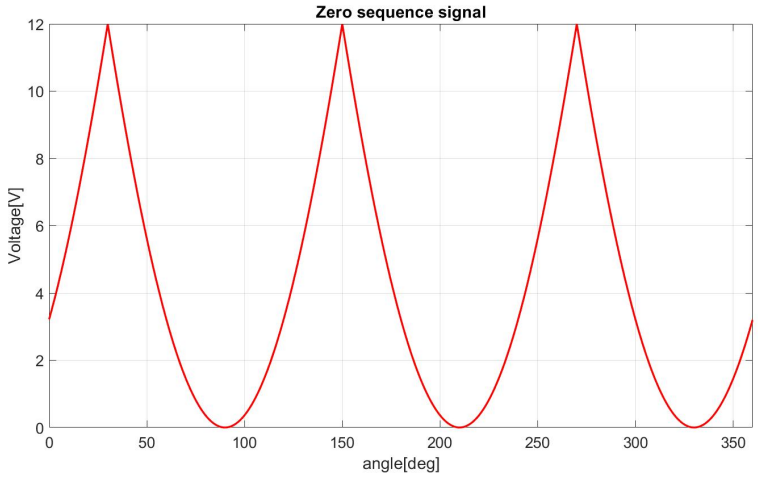

Figure 3.18: Zero sequence signal.

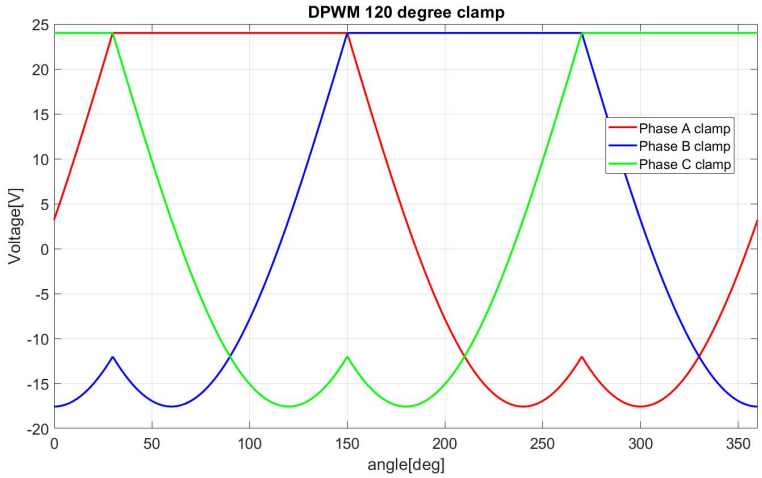

Figure 3.19: DPWM 120 degree clamp signals.

3.1.3.8 DPWM-MIN

This type of technique clamps to the negative rail of the dc bus. The conditions needed for the zero sequence are

$$if \quad |V_{ax}^*| <= |V_{bx}^*|$$

$$and \quad |V_{ax}^*| <= |V_{cx}^*|$$

$$V_{ax}^{**} = sign(V_{ax}^*)\frac{V_{dc}}{2} - V_{ax}^*$$

$$if \quad |V_{bx}^*| <= |V_{ax}^*|$$

$$and \quad |V_{bx}^*| <= |V_{cx}^*|$$

$$V_{bx}^{**} = sign(V_{bx}^*)\frac{V_{dc}}{2} - V_{bx}^*$$

$$if \quad |V_{cx}^*| <= |V_{ax}^*|$$

$$and \quad |V_{cx}^*| <= |V_{bx}^*|$$

$$V_{cx}^{**} = sign(V_{cx}^*)\frac{V_{dc}}{2} - V_{cx}^*$$

The common mode and clamped signals are presented in figure 3.18 and 3.21 respectively.

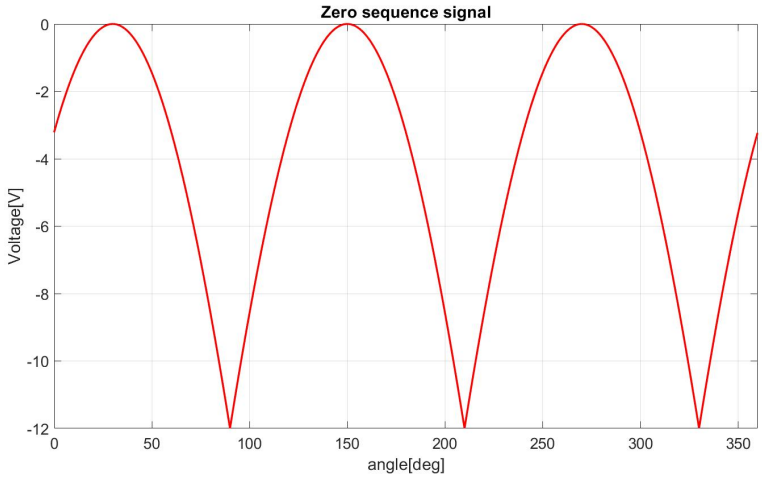

Figure 3.20: Zero sequence signal.

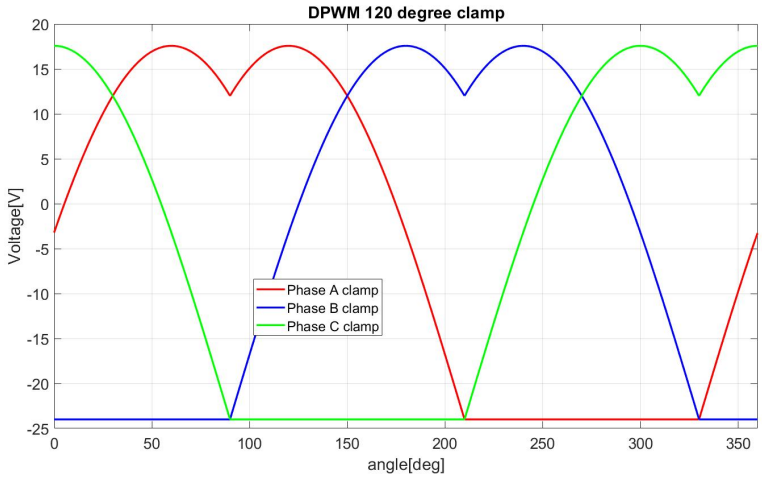

Figure 3.21: DPWM 120 degree clamp signals.

3.1.4 Inverter model

In this section, the inverter model used to generate the required switching signal is demonstrated. The Switches used are insulated gate bipolar transistor, for this simulation ideal characteristics are considered. The model is discretized to work in synchronism with the entire MATLAB model. Since the load to neutral voltage is of interest in this case. Due to the absence of load, the voltage is modeled using relations

$$V_{an} = \frac{2}{3}V_{AN} - \frac{1}{3}(V_{BN} + V_{CN}) \tag{3.15}$$

$$V_{bn} = \frac{2}{3}V_{BN} - \frac{1}{3}(V_{AN} + V_{CN}) \tag{3.16}$$

$$V_{cn} = \frac{2}{3}V_{AN} - \frac{1}{3}(V_{AN} + V_{BN}) \tag{3.17}$$

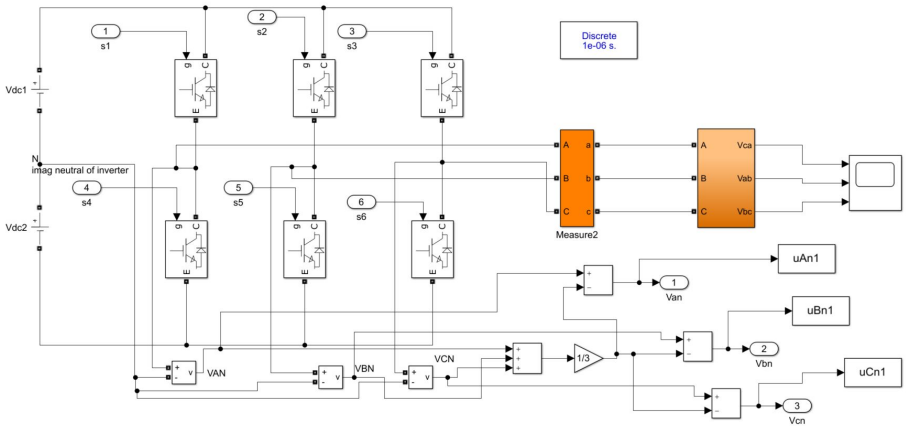

Figure 3.22: IGBT based voltage source inverter model in matlab.

3.2 Ansys Maxwell

Ansys Maxwell is a finite element modeling (FEM) tool that uses numerical methods to determine electric or magnetic field distribution of the structure or model under study. The equations used are known as Maxwell's equations. This tool can be used to obtain a field solution with time-variable fields and also materials that are non-homogeneous, anisotropic, and non-linear. In FEM, the entire analysis is segregated into subdomains, known as finite elements, and then the differential equations are applied to the elements individually.

3.2.1 Permanent magnet machine model in Maxwell 2D

To facilitate a realistic study, a machine model in Ansys is used. The machine model used is a physical based model with materials having non-linear magnetic properties. The design parameters of the machine are described in table 3.4

Table 3.4: Chosen Machine Parameters

Parameters	Values
Dc link Voltage[V]	48
Peak Power[kW]	58
Maximum Torque[Nm]	59.6
$J_{rmsmax}[A/mm^2]$	20
$I_{phrms}[kA]$	1235
Number of stator slots	24
Number of parallel branches	2
Number of winding turns	2
Active length[mm]	80
Poles	8
Air gap length[mm]	0.615
Magnet thickness[mm]	3.73
Magnet width[mm]	59.04
Iron material used	NO30
Magnet material used	NMX-37F

This work aims to be able to extract maximum power from the machine under study. Therefore it is essential to include the saturation of inductance in the machine. As discussed earlier in equation(2.6) L_{sd}, L_{sq} and Ψ_m are an integral part of the torque equation in a permanent magnet machine, so their variation as a function of currents i_{sd} and i_{sq} are also included in this study.

3.2.2 Variation of permanent magnet flux

In this section, the procedure of obtaining the variation of permanent magnet flux linkage Ψ_m is discussed. The method adopted to achieve the magnet flux is evident from (2.3) and (2.4), the i_{sd} component in (2.3) is put to zero and a sweep of the i_{sq} is

done in Ansys Maxwell using an interface called optimetrics which has the capability to sweep different design parameters in the machine. The modified equations are

$$\Psi_q = L_{sq} i_{sq} \tag{3.18}$$

$$\Psi_d = \Psi_m \tag{3.19}$$

It is evident that Ψ_d obtained as a result of the field solution is the Ψ_m and it is a function of the q axis current.The variation is demonstrated in fig 3.23

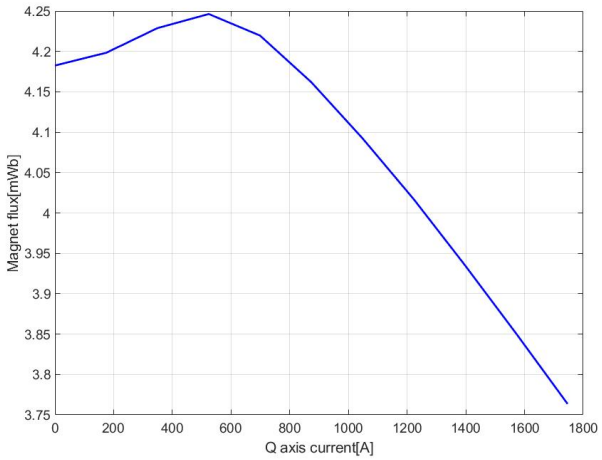

Figure 3.23: Variation of magnet flux with q axis current.

It can be seen that with an increase in i_{sq} current, the magnet flux drops. This variation is used in the later section to compute the direct axis and quadrature axis inductances of the machine.

3.2.3 Variation of inductance in a PM-machine

To be able to do a detailed study, the inductance variation as a function of i_{sd} and i_{sq} is done in this work. The procedure of obtaining the varying inductance in Ansys is to sweep all the possible current angles and the magnitudes of the current vector, this facilitates a combination of the i_{sd} and i_{sq} but the speed is kept fixed as it is deemed that the inductance does not vary with the speed of the machine. The flux linkage obtained from the field solution is post-processed in MATLAB, and the saturation map is obtained, which is demonstrated in figure(3.15) and (3.16).

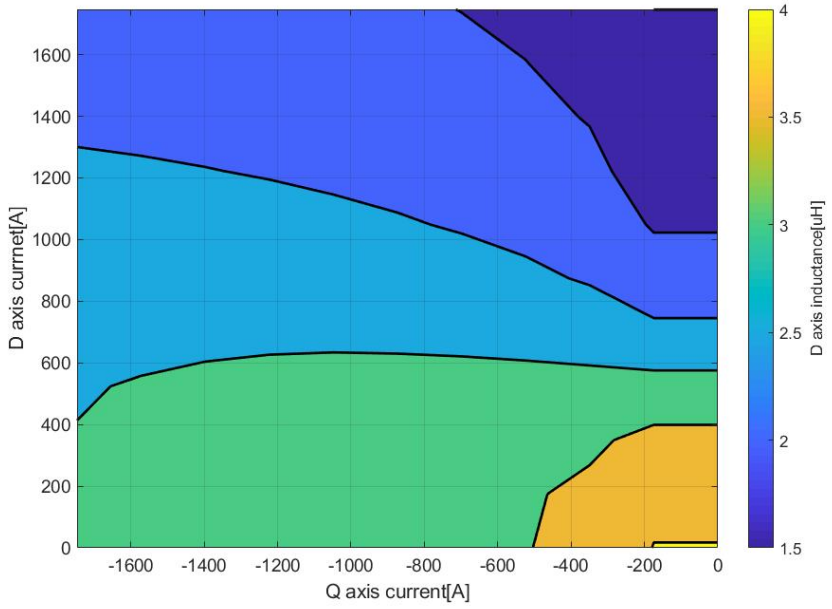

Figure 3.24: Variation of L_{sd} with i_{sd} and i_{sq}current.

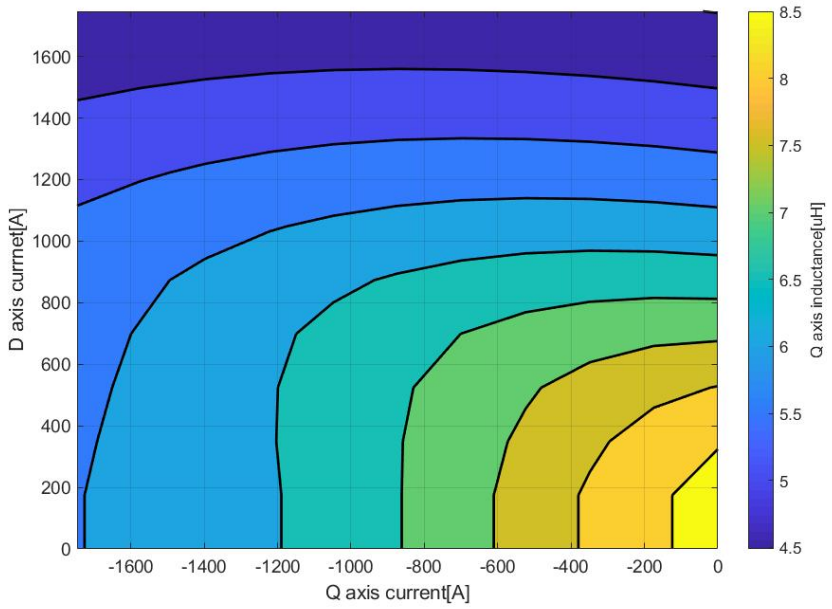

Figure 3.25: Variation of L_{sq} with i_{sd} and i_{sq}current.

The observation made is that the inductance along d axis and q axis saturates with the increase in i_{sd} and i_{sq}. The values obtained are calculcated in the MATLAB model to determine realistic current references. The inductances are dynamically selected in the Simulink model demonstrated earlier along with the magnet flux linkage, this gives a better accuracy to the torque calculated in MATLAB as the model is not physically based instead is a simplified one. The torque obtained from

the calculation is compared to the torque obtained from Maxwell using the same combination of i_{sd} and i_{sq} currents. This comparison is demonstrated in the results section.

4

Results and analysis

4.1 Machine performance

In this section the variation of torque as a function of d and q axis current is demonstrated. The post processed data from Maxwell 2D is illustrated in figure 4.1.

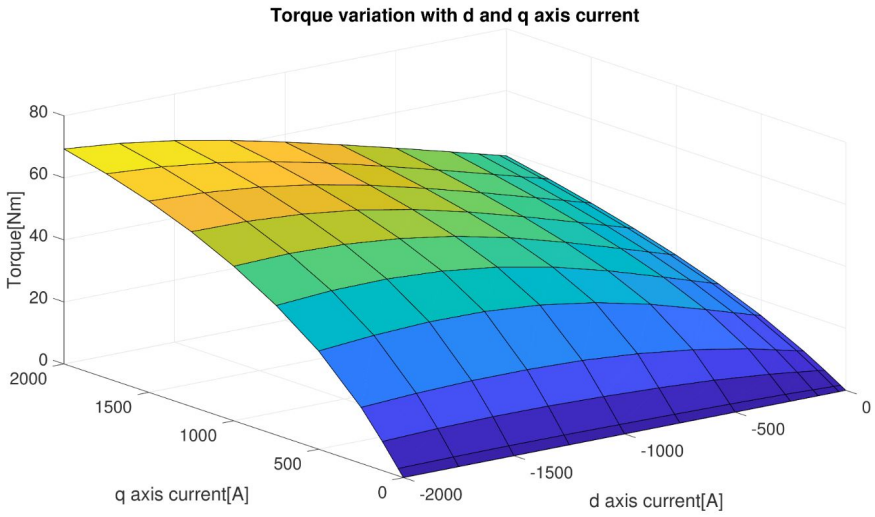

Figure 4.1: Variation of Torque with i_{sd} and i_{sq} current.

The maximum current is limited to 1746.5[A] which can produce a torque of 59.6Nm torque but the sweep of current done is Maxwell to get this data used a maximum current of 2000[A] to facilitate interpolation during post processing data in MATLAB.

4.1.1 Performance of Modulator

The performance of the modulator is defined as the magnitude of fundamental that can be realized by a particular modulator for a particular reference signal. The different degrees of overmodulation, reference voltage magnitude, and fundamental realised are demonstrated in the tabular columns 4.1 and 4.2 where the fundamental voltage for SVM is the same as COVM. The fundamental voltage has an important role to play in the torque-speed mapping, especially in the flux weakening region, where the voltage constraint limits it.

Mod Index	Ref Voltage[V]
1.15	27.6
1.5	36
2.3094	55.426

Table 4.1: Torque Speed Map dependant parameters

It can be observed that the magnitude of fundamental voltage realized by DPMW1 is higher than classical overmodulation, the factors deciding the amount of fundamental is the structure of the zero sequence signal and number of interactions with the carrier waveform. This type of analysis can be done by developing the Fourier series expansion of the saturated waveforms in overmodulation as a function of modulation index, which in turn is a function of the reference signal magnitude.

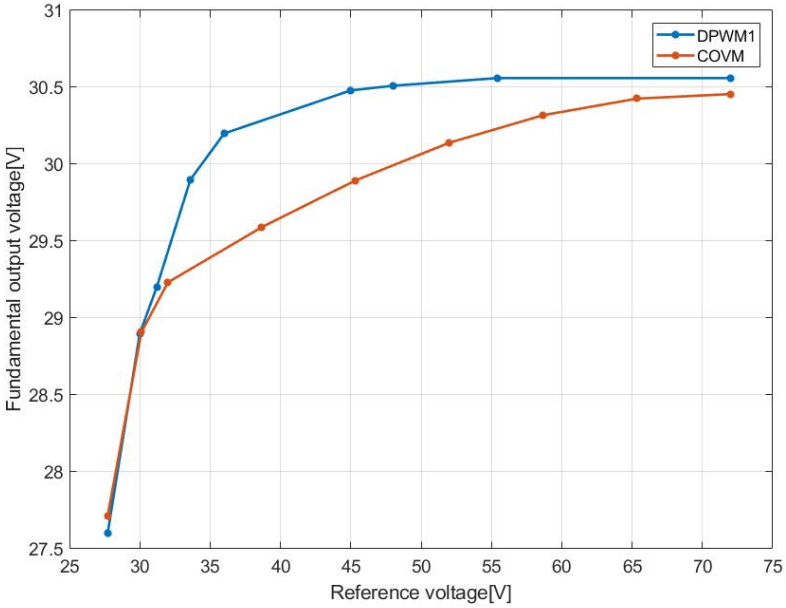

Figure 4.2: Variation of fundemental voltage with modulation index

Mod Index	DPWM1[V]	DPWM0[V]	COVM[V]
1.15	27.6	27.6	27.6
1.5	30.256	29.7	29.7
2.3094	30.55	30.52	30.48

Table 4.2: Variation of fundamental voltage with modulation index

4.1.2 Torque speed mapping

In this section, the torque-speed maps for different degrees of overmodulation are presented. It is to be noted that the different modulation techniques do not influence the torque-speed map. The maps illustrated in figure 4.3a, 4.3b, and 4.4a have different base speeds due to the increasing magnitude of the fundamental component of the phase voltage that is then fed to the electric machine.

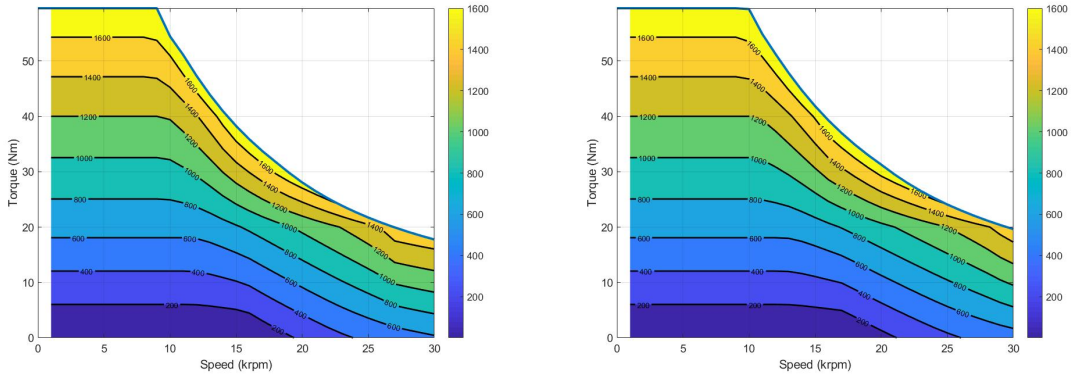

(a) Torque Speed map for dpwm1 with modulation index 1.

(b) Torque Speed map for dpwm1 with modulation index 1.15.

Figure 4.3: Torque Speed map for Modulation Index 1 and 1.15

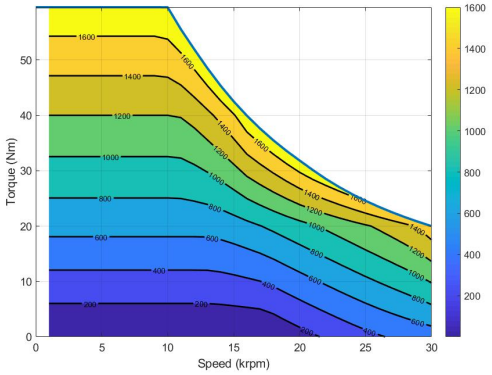

(a) Torque Speed map for dpwm1 with modulation index 1.5.

From the torque-speed maps for various modulation indices, it can be observed that the torque in the voltage-dependent part of the torque-speed characteristics increases

with modulation index, which in turn results in an increase in fundamental voltage. For instance, if the mechanical speed of 20000 rpm is selected there is almost 11% increase in torque from linear modulation range to maximum overmodulation range, this data is to give a feel of the effect of overmodulation on average torque of the machine, the detailed data will be presented in the following sections.

4.1.3 Performance evaluation for 12000 rpm

In this section, the data obtained at post-processing from Ansys Maxwell are presented. The data presented are categorized based on the same fundamental voltage that the different modulation techniques can generate. The fundamental voltage can be backtracked to its reference voltage magnitude and modulation index, respectively, from table 4.1. The comparison in this section is based on three different fundamental voltages, as mentioned in table 4.1, depending on the type of modulation technique used different performance parameters are presented. The operating point of 12000 rpm is used as a reference to validate the performance and behaviour of the machine, therefore the techniques used to evaluate this operating point is only DPWM1 and COVM. A more detailed evaluation is done on the 20000 rpm operating point where DPWM0 is also included.

Table 4.3: Average torque and torque ripple produced at Modulation index of 1.15 for torque request of 47.5[Nm] & speed of 12000[rpm]

Modulation technique	Average torque[Nm]	Torque ripple[%]
COVM	47.18	48.32
DPWM1	47.2	43.85

Table 4.4: Current and Voltage distortion produced at Modulation index of 1.15 for torque request of 47.5[Nm] & speed of 12000[rpm]

Modulation technique	Voltage THD[%]	Current THD[%]
COVM	52.96	7.12
DPWM1	52.8	6.27

Table 4.5: Machine losses Modulation index of 1.15 for torque request of 47.5[Nm] & speed of 12000[rpm]

Modulation technique	Copper Loss[W]	Iron loss[W]	Total Loss[W]	Efficiency[%]
COVM	3200	1035	4235	93.33
DPWM1	3200	1033	4233	93.33

Table 4.6: Average torque and torque ripple produced Modulation index of 1.5 for torque request of 51.4[Nm] & speed of 12000[rpm]

Modulation technique	Average torque[Nm]	Torque ripple[%]
COVM	50.2	69.46
DPWM1	51.37	54.37

Table 4.7: Current and Voltage distortion at Modulation index of 1.5 of 30.02[V] for torque request of 51.4[Nm] & speed of 12000[rpm]

Modulation technique	Voltage THD[%]	Current THD[%]
COVM	41.95	8.02
DPWM1	35.66	6.95

Table 4.8: Machine losses produced at Modulation index of 1.5 for torque request of 51.4[Nm] & speed of 12000[rpm]

Modulation technique	Copper Loss[W]	Iron loss[W]	Total Loss[W]	Efficiency[%]
COVM	3201	1086	4287	93.638
DPWM1	3219	1082	4301	93.753

Table 4.9: Average torque and torque ripple produced at Modulation index of 2.3094 for torque request of 52[Nm] & speed of 12000[rpm]

Modulation technique	Average torque[Nm]	Torque ripple[%]
COVM	51.5	75.8
DPWM1	51.93	75.3

Table 4.10: Current and Voltage distortion produced at Modulation index of 2.3094 for torque request of 52[Nm] & speed of 12000[rpm]

Modulation technique	Voltage THD[%]	Current THD[%]
COVM	31.44	9.01
DPWM1	31.44	8.78

Table 4.11: Machine losses produced at Modulation index of 2.3094 for torque request of 52[Nm] & speed of 12000[rpm]

Modulation technique	Copper Loss[W]	Iron loss[W]	Total Loss[W]	Efficiency[%]
COVM	3226	1120	4346	93.71
DPWM1	3226	1107	4333	93.77

4.1.4 Performance evaluation for 20000 rpm

In this section, the data obtained after post-processing from Ansys Maxwell are presented. The data presented are categorized based on the same fundamental voltage that the different modulation techniques can generate. The fundamental voltage can be backtracked to its reference voltage magnitude and modulation index, respectively, from table 4.1.

Table 4.12: Average torque and torque ripple produced at Modulation index of 1.15 for torque request of 28.17[Nm] & speed of 20000[rpm]

Modulation technique	Average torque[Nm]	Torque ripple[%]
COVM	28.12	102.8
DPWM1	28.11	90.16
DPWM0	28.10	95.2
SVM	28.11	92.5

Table 4.13: Current and Voltage distortion produced at Modulation index of 1.15 for torque request of 28.17[Nm] & speed of 20000[rpm]

Modulation technique	Voltage THD[%]	Current THD[%]
COVM	53.23	8.14
DPWM1	54.2	7.667
DPWM0	54.6	8.13
SVM	52.59	7.89

Table 4.14: Machine losses produced at Modulation index of 1.15 for torque request of 28.17[Nm] & speed of 20000[rpm]

Modulation technique	Copper Loss[W]	Iron loss[W]	Total Loss[W]	Efficiency[%]
COVM	3200	1444	4644	92.6910
DPWM1	3200	1438	4638	92.6974
DPWM0	3200	1440	4640	92.6917
SVM	3200	1442	4642	92.6915

Table 4.15: Average torque and torque ripple produced at Modulation index of 1.5 for torque request of 31.4[Nm] & speed of 20000[rpm]

Modulation technique	Average torque[Nm]	Torque ripple[%]
COVM	30.47	112.83
DPWM1	31.2	107.45
DPWM0	31.07	115.12
SVM	30.48	108.85

Table 4.16: Current and Voltage distortion produced at Modulation index of 1.5 for torque request of 31.4[Nm] & speed of 20000[rpm]

Modulation technique	Voltage THD[%]	Current THD[%]
COVM	45.6	8.52
DPWM1	35.92	7.95
DPWM0	35.6	8.665
SVM	35.6	9.1

Table 4.17: Machine losses produced at Modulation index of 1.5 for torque request of 31.4[Nm] & speed of 20000[rpm]

Modulation technique	Copper Loss[W]	Iron loss[W]	Total Loss[W]	Efficiency[%]
COVM	3201	1459	4660	93.1947
DPWM1	3219	1449	4668	93.3327
DPWM0	3201	1453	4654	93.3113
SVM	3201	1457	4658	93.1995

Table 4.18: Average torque and torque ripple produced at Modulation index of 2.3094 for torque request of 31.9[Nm] & speed of 20000[rpm]

Modulation technique	Average torque[Nm]	Torque ripple[%]
COVM	31.5	120.608
DPWM1	31.77	116.05
DPWM0	31.63	119.307
SVM	31.49	122.23

Table 4.19: Current and Voltage distortion produced at Modulation index of 2.3094 for torque request of 31.9[Nm] & speed of 20000[rpm]

Modulation technique	Voltage THD[%]	Current THD[%]
COVM	31.04	9.909
DPWM1	31.07	9.59
DPWM0	31.05	9.95
SVM	31.05	10.01

Table 4.20: Machine losses produced at Modulation index of 2.3094 for torque request of 31.9[Nm] & speed of 20000[rpm]

Modulation technique	Copper Loss[W]	Iron loss[W]	Total Loss[W]	Efficiency[%]
COVM	3226	1510	4736	93.3114
DPWM1	3226	1491	4717	93.3802
DPWM0	3219	1497	4716	93.3483
SVM	3219	1501	4720	93.3213

4.2 Graphical presentation of performance

In this section, a graphical approach is chosen to present the data obtained from the previous section. A discussion will be made on the behavior of average torque, torque ripple, phase current harmonic distortion, and machine losses. Two speeds i.e. 12000[rpm] and 20000[rpm] have been chosen, and all the performance parameters mentioned above have been analyzed. The speeds determined to belong to the flux weakening region on the torque-speed map and therefore are influenced by the voltage constraint imposed because of inverters maximum voltage capability. The target torque is set to its maximum to obtain the maximum torque for the given speeds since it is already mentioned that in flux weakening region, the torque produced by the machine is a function of the speed.

4.2.1 Analysis of Average torque and Torque ripple

The average torque is seen to be increasing with the increase in modulation index. This behavior of average torque is expected, with the increase in fundamental voltage, due to increased voltage capability from linear modulation to 6-step operation. This is because more current control can be exerted on the machine despite an increase in back emf. The same phenomenon is evident at both speeds demonstrated in figure 4.5a and 4.5b. The torque produced by COVM, SVM and DPWM0 at 1.5 is lesser than DPWM1 at 1.5 because of the less fundamental that can be obtained from COVM, SVM and DPWM0 than DPWM1, which is evident from figure 4.2.

The torque ripple is seen to be more in case of COVM, SVM and DPWM0 than DPWM1, the reason being increased harmonic content in the phase current, which is discussed in the next section, the other factor that is ignored in this work is the back emf distortion as it is also thought have significant effect on torque ripple.

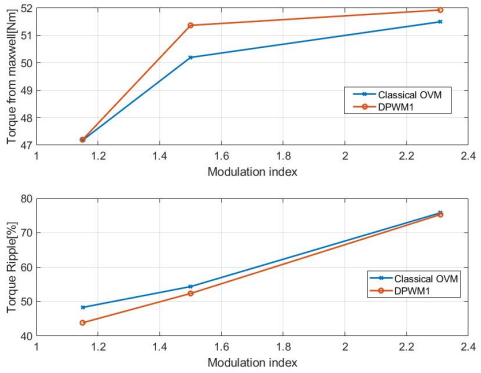

(a) Variation of torque with modulation index at 12000 rpm.

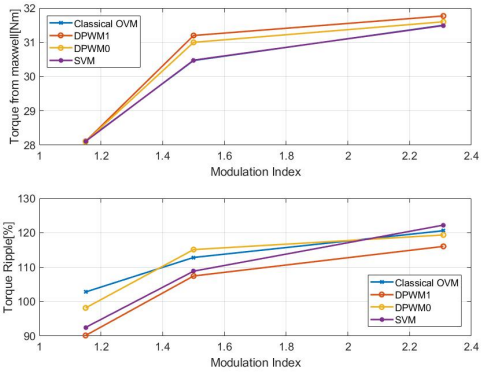

(b) Variation of torque with modulation index at 20000 rpm.

Figure 4.5: Variation of torque with modulation index

4.2.2 Analysis of Total harmonic distortion

It is of equal importance to analyze the harmonic content or distortion in the phase current since that conveys information about the torque ripple. From the figure 4.6a and 4.6b it can be observed that from linear modulation maximum range to 6-step operation there is an increase in phase current THD content and that is because of the appearance of the lower order harmonics in the spectrum.

The phase voltage distortion is as expected, and it is least in case of 6-step operation because of the least number of switching occurring in a period, which in turn means lesser interaction with the carrier waveform.

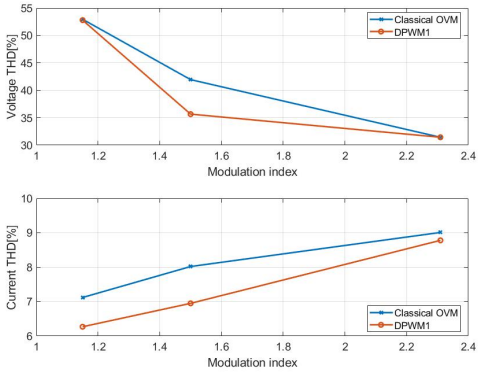

(a) Variation of THD with modulation index at 12000 rpm.

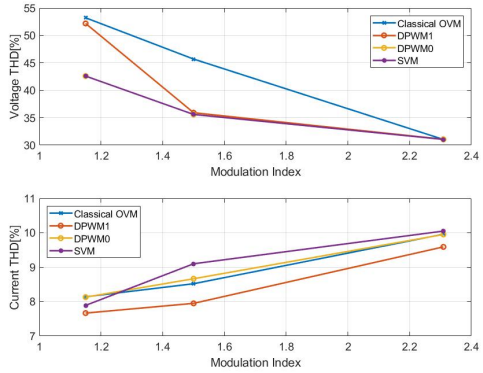

(b) Variation of THD with modulation index at 20000 rpm.

Figure 4.6: Variation of THD with modulation index

4.2.3 Analysis of reference and fundamental voltage

This section is of prime importance as it aids in validating figure 4.2, the fundamental attained by a certain modulator is evaluated based on a FFT algorithm in MATLAB. It is evident from figure 4.7a and 4.7b that the fundamental realisation capability of DPWM1 and COVM, SVM and DPWM0 are very different. When in linear modulation range, the reference voltage and the fundamentals are exactly similar, but when pushed into the overmodulation region COVM, SVM and DPWM0 has lesser capability than DPWM1 in terms of fundamental voltage realization. This capability of the modulator depends on the type of zero sequence signal injected and also on the interactions with the carrier signal. The exact values of the reference voltage and their respective fundamental voltages can be found in table 4.1 and 4.2, respectively.

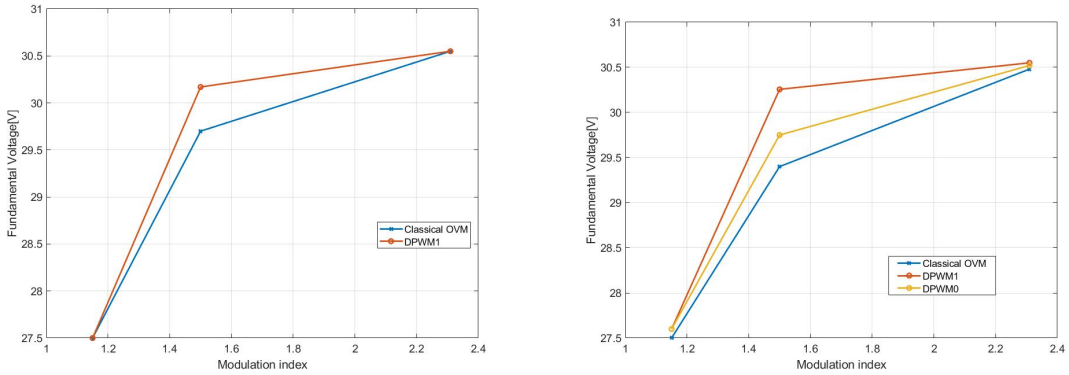

(a) Variation of reference and fundamental with modulation index at 12000 rpm.

(b) Variation of reference and fundamental with modulation index at 20000 rpm.

Figure 4.7: Variation of reference and fundamental with modulation index

4.2.4 Analysis of Machine Losses

Machine losses are decomposed into two components the copper loss and the iron loss. The copper loss is dependant on the current magnitude. The current magnitude is kept the same for a particular modulation index as can be observed from figure 4.8 where the COVM and SVM curve is overlapped with DPWM0. The current magnitude should theoretically be 1746[A] but since an open loop control is used and on the other hand the machine model is fed with PWM patterns, it becomes challenging to realize the theoretical current.The current magnitudes used for DPWM1 is higher than the other two techniques because of the higher fundamental voltage realised, the current magnitudes of DPWM0, SVM and COVM are kept the same as the fundamental voltage generated by these three techniques are almost the same. A sweep of voltage angles is done to get a torque that satisfies both the current and voltage constraint.

In case of iron loss, it is of interest to notice that iron loss increases with an increase in fundamental voltage and the phenomenon can be seen from figures 4.9 and

4.10. The reason can be found in the section 2.3.2.2, where the dependency of core loss on fundamental voltage has been established, though the current magnitude and current angle may have an effect on the iron loss to a certain extent it is not considered in this work. The factors considered in this work are back emf distortion, which is related to the flux density and its harmonic content and are believed to have a significant effect on core losses in the machine.

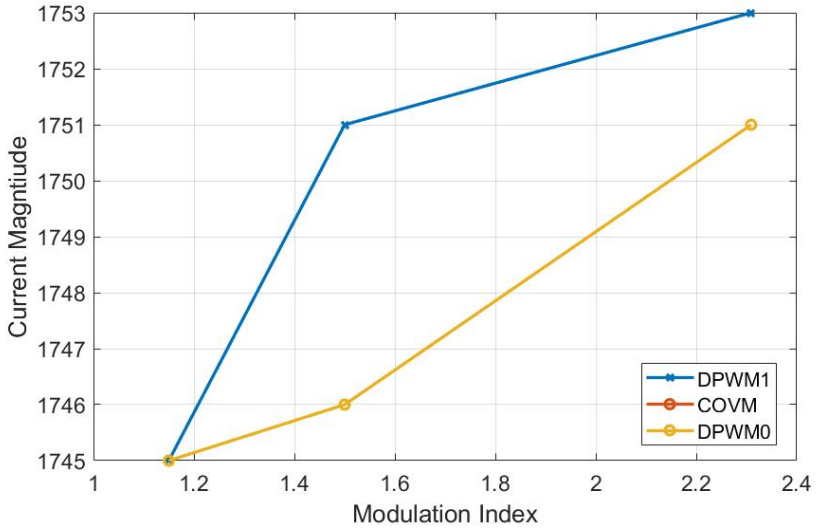

Figure 4.8: Variation of Current magnitude with Modulation Index .

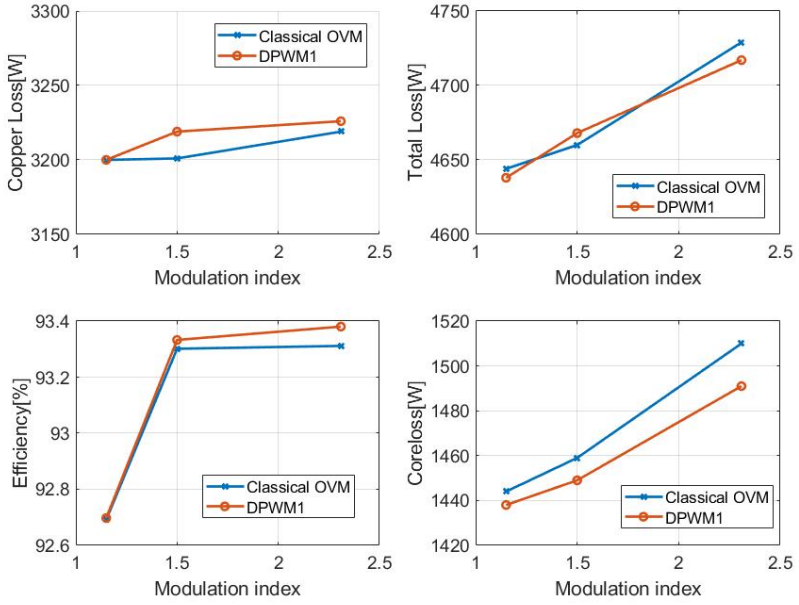

Figure 4.9: Variation of Machine losses with Modulation Index at 12000[rpm].

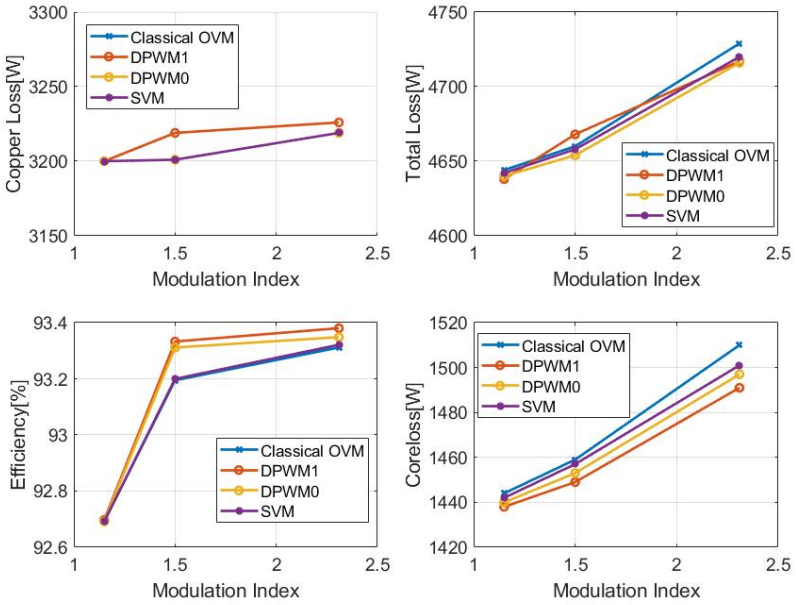

Figure 4.10: Variation of Machine losses with Modulation Index at 20000[rpm].

4.3 Inverter Loss

The inverter loss maps are highly dependant on the type of modulation technique used, the switching frequency, current magnitudes, and power factor. The switching frequency used in this section for evaluation is an odd integer multiple of the fundamental frequency. For this work the value chosen is 13, other integers commonly used are 9,11 and 21[6], 21 is not used since the speed operating point of interest is 20000 rpm which will result in a very high switching frequency, given that the machine operates with kiloamps, so it was decided it would not be realistic to switch such high currents at a very high switching frequency.

The tables 4.21, 4.22 and 4.23 present the inverter loss data in terms of conduction loss, switching loss and total inverter loss for different modulation techniques and also different modulation indices.

Table 4.21: Inverter losses produced at Modulation index of 1.15 for torque request of 28.17[Nm] & speed of 20000[rpm]

Modulation technique	Conduction Loss[W]	Switching Loss[W]	Total Loss[W]
COVM	1062	562	1624
DPWM1	1059	384.4	1443.4
DPWM0	1053	478.5	1531.5

Table 4.22: Inverter losses produced at Modulation index of 1.5 for torque request of 31.4[Nm] & speed of 20000[rpm]

Modulation technique	Conduction Loss[W]	Switching Loss[W]	Total Loss[W]
COVM	1131	578.5	1709.5
DPWM1	1144	395.5	1539.5
DPWM0	1136	495.5	1631.5

Table 4.23: Inverter losses produced at Modulation index of 2.3094 for torque request of 31.9[Nm] & speed of 20000[rpm]

Modulation technique	Conduction Loss[W]	Switching Loss[W]	Total Loss[W]
COVM	1144	584	1728
DPWM1	1144	398	1542
DPWM0	1144	497	1641

4.3.1 Graphical evaluation of inverter loss

In this section, an analysis is done on the inverter loss phenomenon in the overmodulation region. As is evident, the conduction loss is almost the same in terms

of magnitude for both modulation techniques of DPWM1, DPWM0 and COVM, that is expected because the conduction loss does not depend on the power factor. The switching loss is the deciding factor of the inverter loss map. COVM has more switching loss as it is a continuous PWM technique whereas DPWM1 and DPWM0 are discontinuous techniques with a reduced number of commutations, which aids in lowering the switching loss of the inverter. The variation of the inverter loss and its components as a function of speed and torque is demonstrated in the next section.

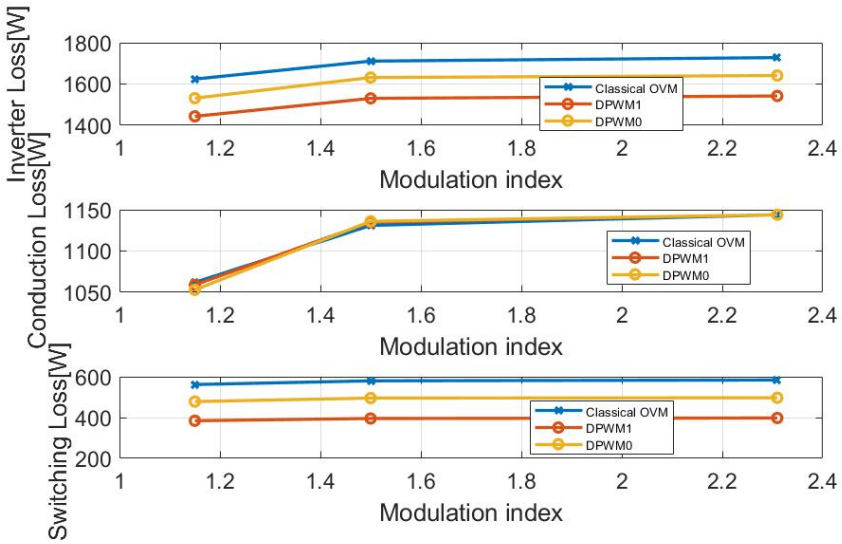

Figure 4.11: Variation of Inverter losses with Modulation Index at 20000[rpm].

4.3.2 Conduction Loss in inverter

The conduction losses for different modulation techniques doesn't differ much as the operational points and the power factor are the same. This might seem contradictory since the switching patterns for SVM and DPWM are different. However, during one switching period, the same active and zero vectors are applied for both techniques and the time applied on those vectors are also the same. Only the order in which they are applied is different[5].

4.3.3 Switching loss in inverter

In this section, the switching loss maps for different modulation technique are presented. The switching loss is the more critical loss component for inverter loss determination. The switching loss maps for SVM and COVM are dealt with together as they were deemed to have the same conduction and switching loss as both the techniques result in the same reference voltage after zero sequence injection but the way of implementation is different. The switching loss for DPWM techniques is highly dependant on the current magnitude being switched, degree and position of clamping and the power factor. But on the other hand, for continuous PWM it is highly dependant on the current magnitude. Since a variable switching frequency is utilized, thereby, it can be observed that the loss magnitude continues increasing with increasing speed. For the evaluation of switching loss for DPWM, the technique of SLF is used.

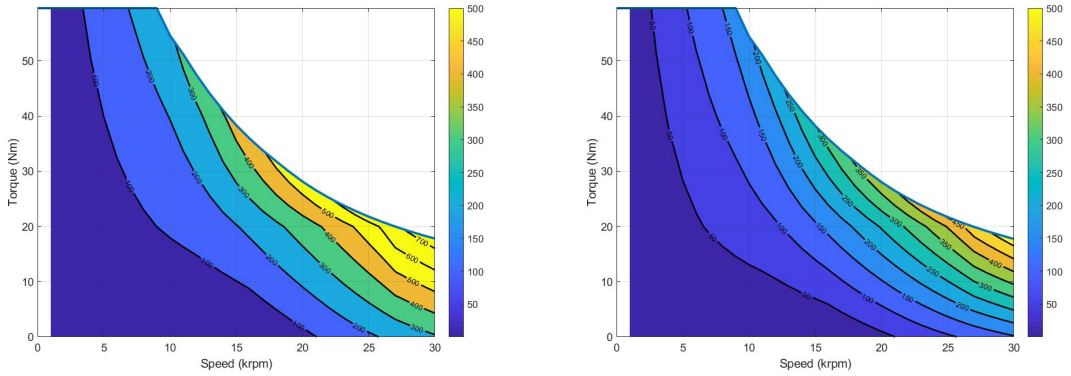

(a) Switching Loss for COVM with modulation index 1.15.

(b) Switching Loss for DPWM1 with modulation index 1.15.

Figure 4.12: Switching Loss map for Modulation Index 1.15

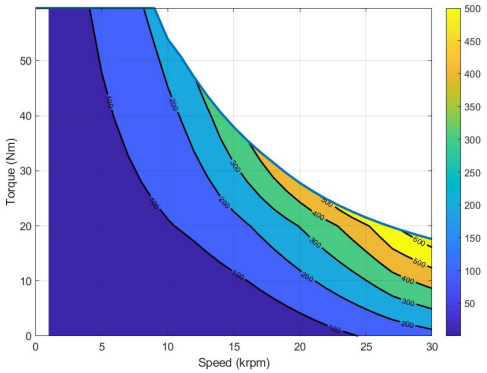

(a) Switching Loss for DPWM0 with modulation index 1.15.

Figure 4.13: Switching Loss map for Modulation Index 1.15

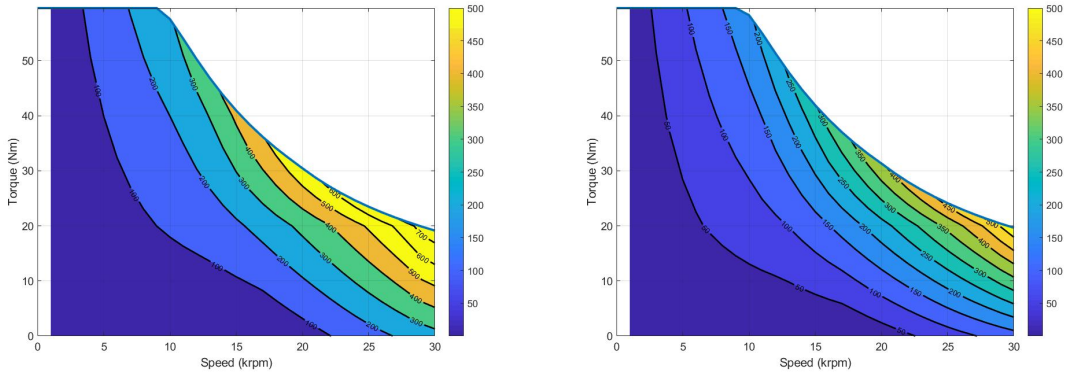

(a) Switching Loss for COVM with modulation index 1.5.

(b) Switching Loss for DPWM1 with modulation index 1.5

Figure 4.14: Switching Loss map for Modulation Index 1.5

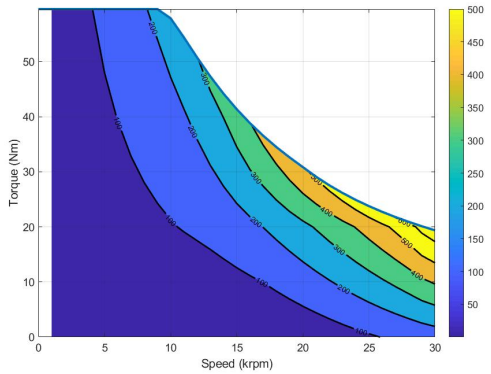

(a) Switching Loss for DPWM0 with modulation index 1.5

Figure 4.15: Switching Loss map for Modulation Index 1.5

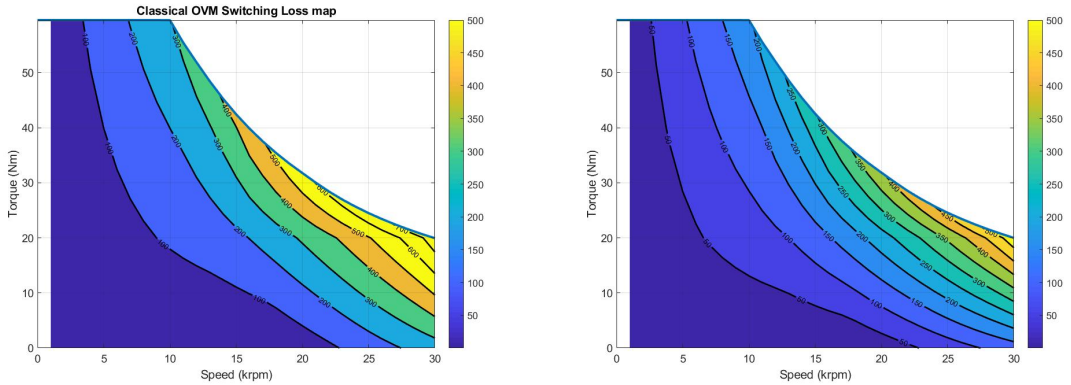

(a) Switching Loss for COVM in 6-Step operation

(b) Switching Loss for DPWM1 in 6-Step operation

Figure 4.16: Switching Loss map for 6-Step operation

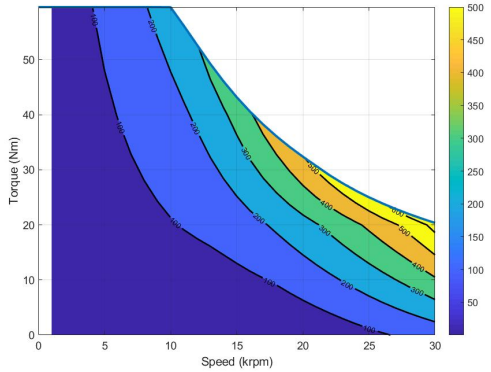

(a) Switching Loss for DPWM0 in 6-Step operation

Figure 4.17: Switching Loss map for 6-Step operation

4.3.4 Total Inverter Loss

In this section, the total inverter loss for the three techniques is evaluated, and the losses as a function of the torque-speed map are presented in figures 4.18a, 4.18b, 4.19a, 4.20a, 4.20b,4.21a, 4.22a, 4.22b and 4.23a.

It can be observed that COVM being a continuous PWM technique incurs higher losses in terms of switching loss, whereas DPWM1 and DPWM0 proves to be advantageous due to reduced commutations and thereby lower switching losses, the difference between DPWM1 and DPWM0 being the position of the clamping in a fundamental period.

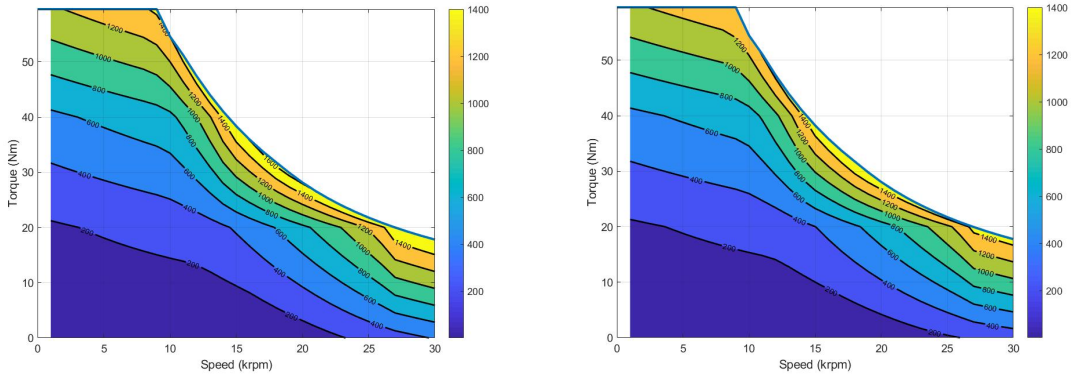

(a) Total Loss for COVM with modulation index 1.15.

(b) Total Loss for DPWM1 with modulation index 1.15.

Figure 4.18: Total Loss map for Modulation Index 1.15

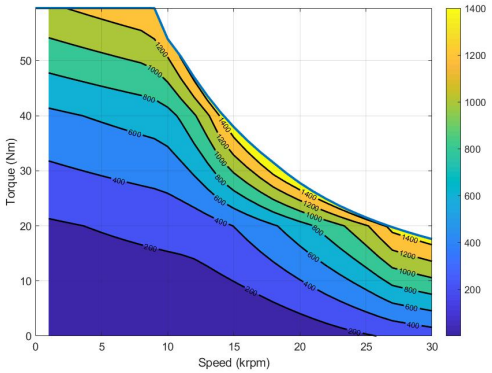

(a) Total Loss for DPWM0 with modulation index 1.15.

Figure 4.19: Total Loss map for Modulation Index 1.15

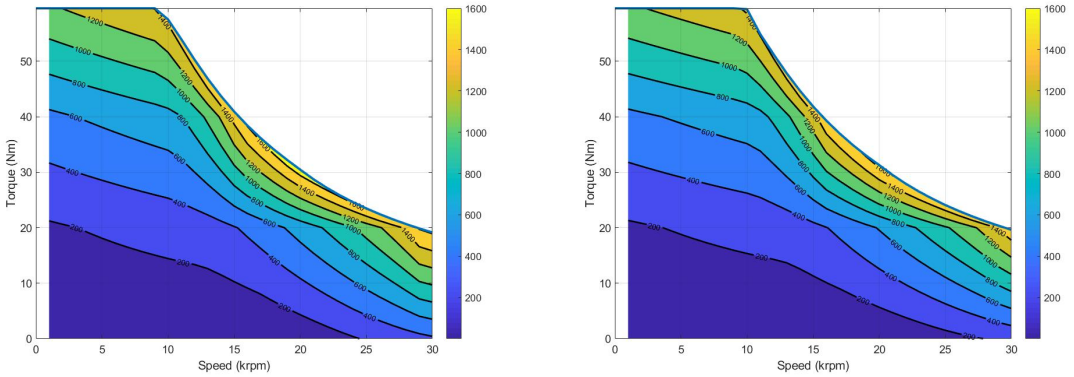

(a) Total Loss for COVM with modulation index 1.5.

(b) Total Loss for DPWM1 with modulation index 1.5

Figure 4.20: Total Loss map for Modulation Index 1.5

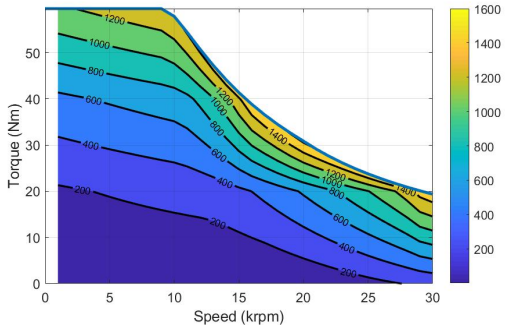

(a) Total Loss for DPWM0 with modulation index 1.5

Figure 4.21: Total Loss map for Modulation Index 1.5

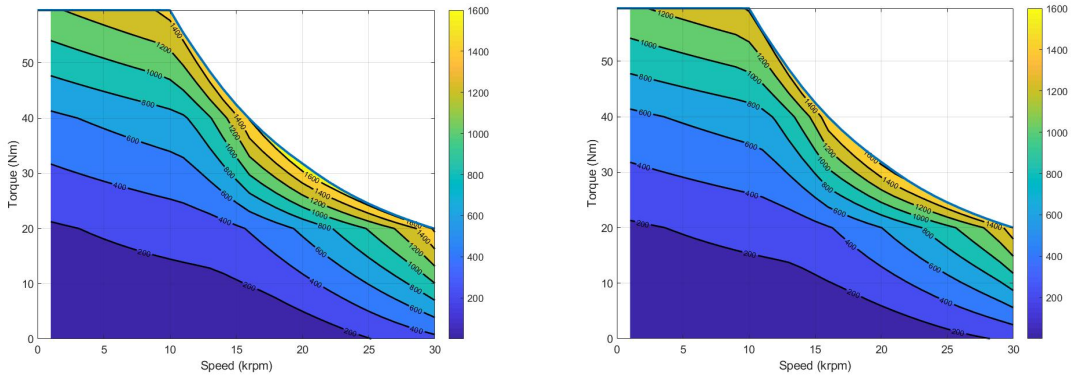

(a) Total Loss for COVM in 6-Step operation

(b) Total Loss for DPWM1 in 6-Step operation

Figure 4.22: Total Loss map for 6-Step operation

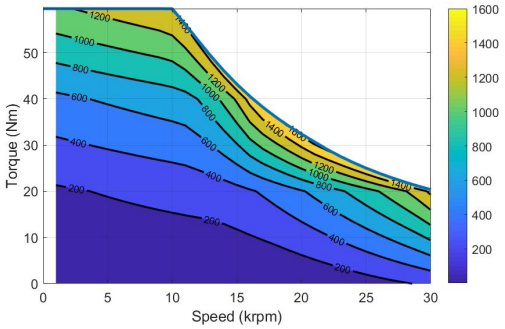

(a) Total Loss for DPWM0 in 6-Step operation

Figure 4.23: Total Loss map for 6-Step operation

4.3.5 Relative discrepancy in inverter loss

In this section, the discrepancy in the switching loss and total inverter loss for the three different modulation techniques is evaluated. The discrepancy is evaluated using the relation

$$P_{discrepancy} = P_{COVM} - P_{DPWM1} \tag{4.1}$$

$$P_{discrepancy} = P_{COVM} - P_{DPWM0} \tag{4.2}$$

The evaluation is made considering COVM as the base. This section elucidates on the increased switching loss in COVM when compared to DPWM1 and DPWM0. The maps presented in figures 4.24a, 4.24b, 4.25a, 4.26a, 4.26b and 4.27a are a function of power factor, degree of clamping in the DPWM technique adopted and the magnitude of current. It is found that in terms of losses DPWM1 has better performance than the other two techniques.

4.3.5.1 Relative discrepancy in total inverter loss for DPWM1 and DPWM0

The conclusions derived in the previous section applies to this section. Since the conduction loss is considered to be almost the same, the discrepancy in the total inverter loss maps is dictated by the switching loss incurred by the modulator.

It can be observed that a considerable amount of energy is saved when using DPWM1 or DPWM0 over COVM, The energy saving for DPWM1 is found to be almost twice of DPWM0, the reason being power factor, as the operating power factor of the machine decides the amount of energy saved.

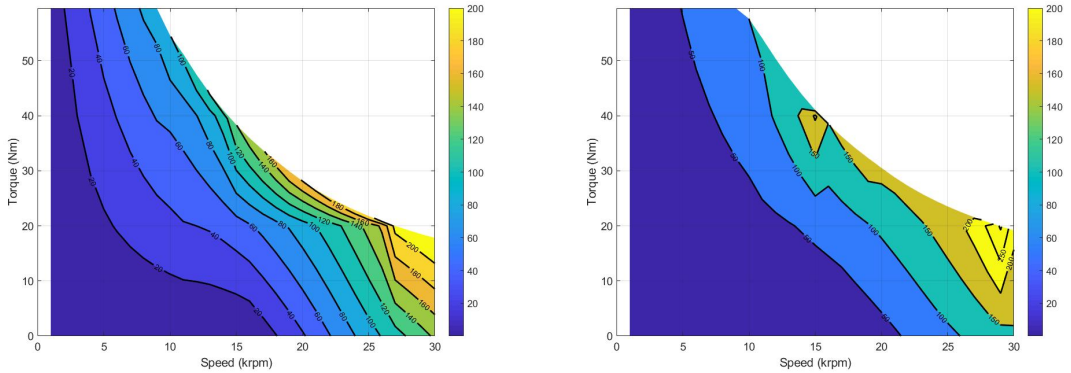

(a) discrepancy in total inverter loss for modulation index 1.15 for DPWM1

(b) discrepancy in total inverter Loss for modulation index 1.5 for DPWM1

Figure 4.24: Inverter Loss map for Modulation Index 1 and 1.15

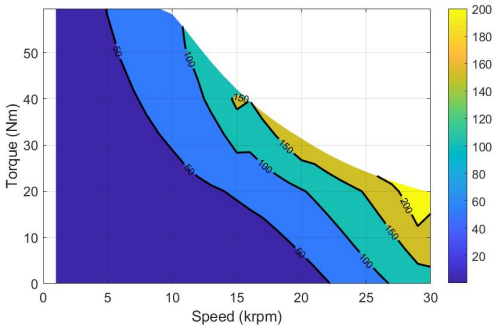

(a) discrepancy in total inverter Loss for modulation index 2.3094 for DPWM1

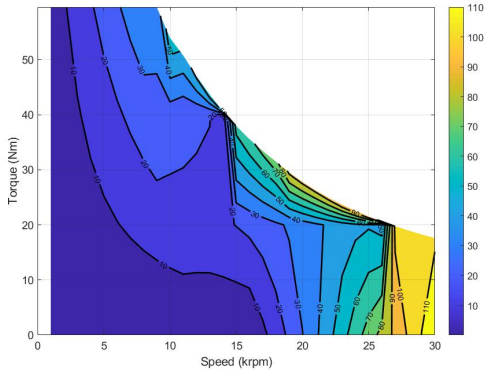

(a) discrepancy in total inverter loss for modulation index 1.15 for DPWM0

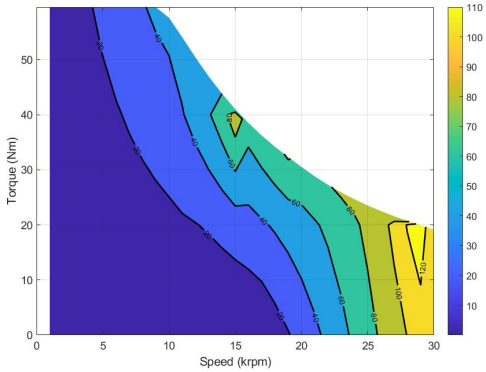

(b) discrepancy in total inverter Loss for modulation index 1.5 for DPWM0

Figure 4.26: Inverter Loss map for Modulation Index 1 and 1.15

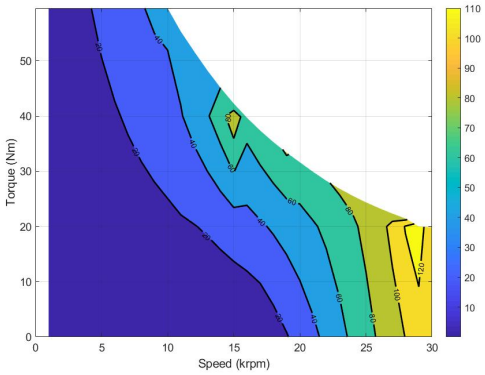

(a) discrepancy in total inverter Loss for modulation index 2.3094 for DPWM0

4.4 Comparative analysis of parameters

In this section, the variation of torque with core loss, current THD and switching loss for three different modulation techniques is evaluated. From figure 4.28 it can be observed that the core loss increase with torque increasing, mainly caused by back-emf distortion as mentioned in section 4.2.4, where COVM has the highest loss compared to SVM, DPWM1 and DPWM0.

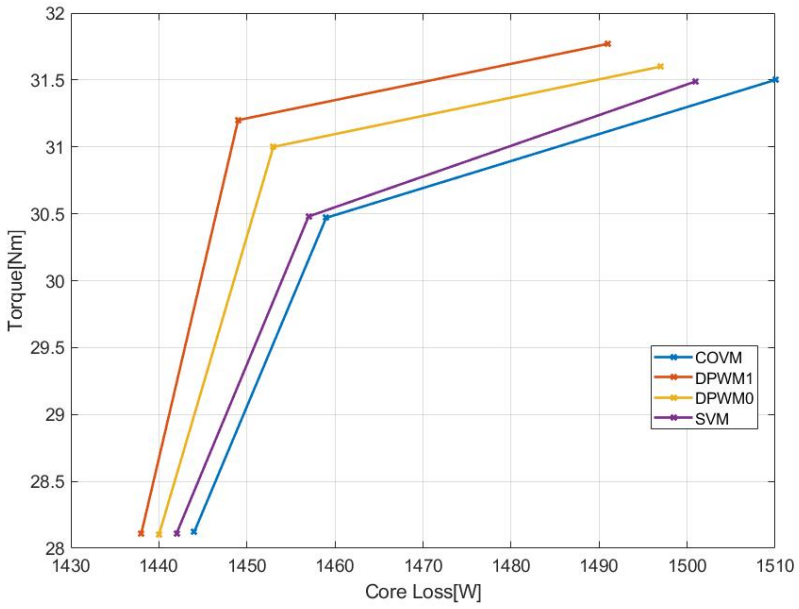

Figure 4.28: Variation of Torque with Core loss at 20000[rpm].

Figure 4.29 shows that the current THD also increased with torque due to the appearance of the lower order harmonics, where DPWM1 has the least current THD.

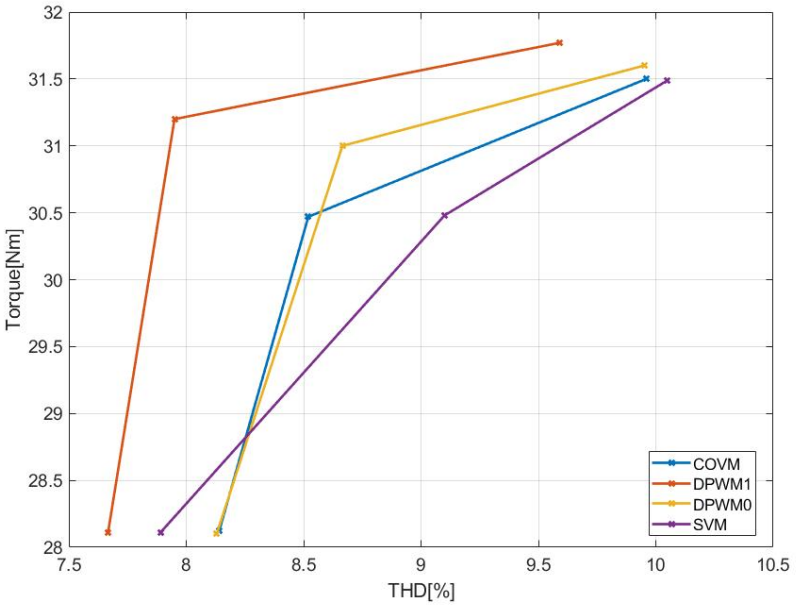

Figure 4.29: Variation of Torque with Current THD at 20000[rpm].

Figure 4.30 shows that torque increase also bring an increase in switching loss with an increased current magnitude, where COVM has the highest loss and DPWM1 has the lowest loss.

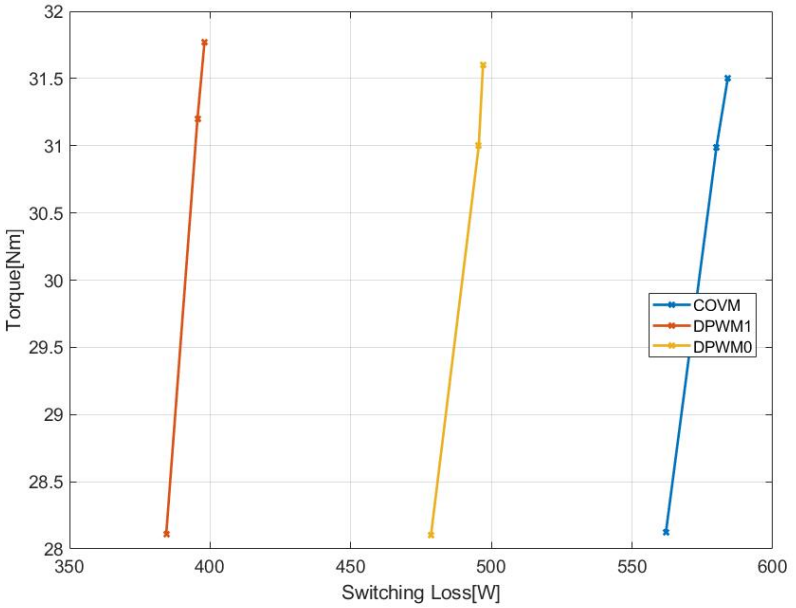

Figure 4.30: Variation of Torque with Switching loss at 20000[rpm].

5

Conclusion

In this thesis work, a comparison of different modulation techniques, their performance, and drawbacks have been analysed and discussed.

In chapter 2, the underlying concepts of electric machine control in steady state is discussed, as that forms an integral part of the work. The base on overmodulation is devised, and different modulation strategies based on continuous PWM techniques and discontinuous PWM techniques are presented. The performance evaluation section comprises of performance parameters in an electric machine as well as an inverter, parameters like extra torque, machine losses(core losses), harmonic distortion and inverter losses are used to analyse the performance of the modulator.

In chapter 3, the implementation of the different types of modulator that are to be analysed has been presented. It also includes the implementation of some of the discontinuous clamping techniques which have not been utilised in this work. In this section the finite element modelled machine, and its inductance mapping is also discussed, as it is of prime importance to represent a physical, non-linear electric machine in the steady-state control algorithm, to have realistic reference currents.

In chapter 4, the performance of the modulator, as discussed in chapter 2, is presented. The primary objective in this work was to push to the modulator to 6-Step operation and validate the increase in torque using a finite element modelled electric machine. A sweep of the modulation index is done, and it is observed that in the flux weakening region where the voltage constraint is active, there is a significant increase in the average torque. The increase in torque is 13.7% for dpwm1, 12.56% for dpwm0 and 12.02% for covm and svm, at a speed of 20000 rpm and 10% for dpwm1 and 9.1% for covm at 12000 rpm. In terms of the fundamental realised most techniques behave differently, dpwm1 has a better DC bus utilisation in terms of fundamental voltage as compared to covm, as can be observed from figure 4.2, which forms the base of the increased average torque from a modulator that uses dpwm1. The harmonic performance of dpwm1 for each modulation index analysed is also lower than dpwm0 and covm for 12000 rpm and 20000 rpm, which results in a better torque ripple performance from the machine. In the case of machine losses, the copper losses were evaluated based only on the fundamental component of the current magnitude and was kept unchanged for a particular modulation index, this made the analysis of total loss of the machine dependant on the core loss which is a function of the flux density, current angle, and current magnitude. Since an

analytical estimation of core loss would add complexity, the FEM package is trusted for the values of iron losses. There was an increased loss for covm , svm and dpwm0 over dpwm1 in all the cases analysed. It has been developed in chapter 2, that dependency of core loss can be proposed in terms of fundamental voltage and its RMS value, which could explain such a behaviour. But it is equally important to analyse the flux density harmonic content to be able to explain the core loss behaviour. Inverter losses are deemed to be an important parameter for the analysis of the modulator. The base has been built in chapter 2; the dpwm1 and dpwm0 was found to be advantageous to use, because of reduced commutations occurring in a half cycle of the fundamental period, dpwm1 and dpwm0 proved to have lower switching losses than covm and svm in the flux weakening region. But dpwm1 was found to have better performance than dpwm0 when the two discontinuous pwm techniques were analysed. The discrepancy plots for inverter losses also exhibit the fact that the dpwm techniques rely a lot on the machine power factor and current magnitude than inverter losses of continuous methods wherein it is reliant on current magnitude solely.

It is particularly challenging to identify one modulator with enhanced performance in the entire torque speed map of an electric machine, though the dpwm1 has exceptionally higher fundamental voltage realisation capability than other discontinuous techniques. The selection criteria also involves power factor and harmonic distortion range that is acceptable. As is suggested in literature [14], a combination of modulators could be an approach as covm performs better in lower modulation range and dpwm1 performs better in higher modulation range. The preferable choice in the overmodulation range is dpwm1 over dpwm0, svm and covm.

6
Sustainability

6.1 Sustainability aspects

In this section, a comparison of the battery electric vehicle will be made with a conventional combustion vehicle based on ecological, economic and social aspects. Electrification of vehicles has gained importance in recent times. One of the key factors in progressing towards vehicular electrification has been the increasing emissions, which in turn has detrimental effects on the environment. This thesis work aims at enhancing the performance of an electric vehicle, which is a better alternative to a conventional combustion vehicle.

6.1.1 Ecological aspects

In case of battery electric vehicles(BEV), which comprises of electric machines, power electronics, and a battery pack, do not contribute to any emission during opeartion that harms the environment which is not the case for a combustion vehicle. According to the EU commission, from 2021, the EU fleet-wide average emission target for new cars will be 95 g CO2/km. The average emissions of all newly registered cars of a manufacturer will have to be below the target [15]. This emission level corresponds to a fuel consumption of around 4.1 l/100 km of petrol or 3.6 l/100 km of diesel [15]. The conventional combustion vehicle has been responsible for a more significant part of the air quality degradation, but it is to be noted that, the majority of electrical power generation still uses fossil fuels such as coal or natural gas, which also contributes to the air pollution. Advancements in the fields of renewable sources of energy like wind, solar, tidal, geothermal, and hydropower have led to a significant mitigation of air quality degradation when it comes to the production of power.

The main impact of a BEV on an ecological scale is the usage of rare earth materials in the propulsion system. The primary energy storage used is generally a battery pack, lithium is a fundamental metal used in these battery packs. When it comes to the electric machines, the most commonly used is a permanent magnet synchronous machine which as the name suggests uses rare earth magnets. The usage of these aforementioned rare earth materials makes sustainable production of electrified vehicles challenging. The mining of these metals contribute significantly to the air quality decline, and another essential factor is the working condition of workers in these mines, as they are exposed to harmful radiations which affect their life adversely.

The solution to the problems has led to more research and development in areas of electric machines where other suitable competitors would be induction machines or synchronous reluctance machines. The PMSM offers higher efficiency and power density when compared to the alternatives, which implies that the pm machine is more compact and saves weight in the car. But with advancements in electric machine design, performance criteria can be met with the usage of lesser magnets.
To sum it up, electric machines have much higher working efficiency when compared to combustion vehicles and last but not the least, is the energy recovery during braking. All these factors give an extra edge to a BEV over a conventional combustion vehicle.

6.1.2 Economical aspects

Due to the usage of rare earth metals like neodymium and lithium, the initial cost of a BEV vehicle is more expensive than a combustion vehicle. The advancements in battery technology have led to a decrease in value significantly over the years making it viable for manufacturers as well as customers.

The fuel cost of combustion vehicles is also higher than the price of electricity. The efficiency gained from the use of the electric vehicle over combustion also affects the operating cost of the car during its lifetime.

The alternatives to PMSM i.e. IM and synchronous reluctance machine might be more beneficial in terms of sustainability. It is to be noted that neodymium, the rare earth material used in a permanent magnet machine is mainly found in China. Therefore the extraction from mines and production are also controlled by them, implying the dependency of several countries on China. According to data from China Customs, China's exports of NdFeB permanent magnets increased 11% in 2018. The nation exported NdFeB magnets to 104 countries in 2018, down from 109 the year prior [16]. The value of China's NdFeB exports increased 14% and the sales-weighted average unit price increased 3%, from US 49.14$ per kilogram to the US 50.40$ per kilogram [16] .

6.1.3 Social aspects

Electric vehicles are way quieter than combustion vehicle, which make them more viable in transportation, especially in the city area. The higher power density, higher efficiency implies a lesser volume of the machine and lower size of the battery, which means more space in the car.

The drawback of using permanent magnet machines is the use of permanent magnets, which are extracted from mines. These mines have adverse working conditions with workers getting exposed to harmful radiations, making it a not so healthy working environment for workers.

From a safety perspective, the pmsm can continue to induce voltage into the system even though the machine is shut down due to the presence of magnets in the rotor. This aspect is seen as an advantage for an IM as the rotor excitation can be controlled.

In a nutshell, combining all the positives from a battery electric vehicle, the reduced emission, more efficiency, lesser maintenance, lesser operating cost lead to a strong argument in favor of the BEV over ICE. But steps should be taken to improve the work environment in the mines by imposing better rules and regulation for workers in the mines and making the extraction process automated.

Bibliography

[1] C. Capitan, "Torque Control in Field Weakening Mode", no. June, p. 84, 2009.

[2] A. Kronberg, "Design and Simulation of Field Oriented Control and Direct Torque Control for a Permanent Magnet Synchronous Motor with Positive Saliency", *Design and Simulation of Field Oriented Control and Direct Torque Control for a Permanent Magnet Synchronous Motor with Positive Saliency*, pp. 2–38, 2012, ISSN: 02671379 (ISSN). DOI: 10.1097/MOG.0b013e3282c8c8d3.

[3] T. Dalgleish, J. M. G. Williams, A.-M. J. Golden, N. Perkins, L. F. Barrett, P. J. Barnard, C. Au Yeung, V. Murphy, R. Elward, K. Tchanturia, and E. Watkins, "[Electric Machinery Fundamentals]", *Journal of Experimental Psychology: General*, vol. 136, no. 1, pp. 23–42, 2007.

[4] A. Opritescu, "Control of a Saturated Permanent Magnet Synchronus Motor", *Master Thesis, Aalborg University*, 2010.

[5] A. Andersson, "Electric machine control for energy efficient electric drive systems", 2015.

[6] D. G. Holmes and T. A. Lipo, *Pulse Width Modulation for Power Converters*. 2003, ISBN: 9780470546284. DOI: 10.1109/9780470546284. [Online]. Available: http://ieeexplore.ieee.org/xpl/bkabstractplus.jsp?bkn=5264450.

[7] A. M. Hava, R. J. Kerkman, and T. A. Lipo, "Carrier-based PWM-VSI overmodulation strategies: Analysis, comparison, and design", *IEEE Transactions on Power Electronics*, vol. 13, no. 4, pp. 674–689, 1998, ISSN: 08858993. DOI: 10.1109/63.704136.

[8] A. O. Algorithm, " ", pp. 3–8, 2010. DOI: 10.19595/j.cnki.1000-6753.tces.2010.01.010.

[9] A. M. Hava, S. Member, R. J. Kerkman, and T. A. Lipo, "A High-Performance Generalized Discontinuous PWM Algorithm", no. January, 1998.

[10] K. J. Tseng and S. Ieee, "Analysis of Flux Distribution and Core Losses in Interior Permanent Magnet Motor", vol. 14, no. 4, pp. 969–975, 1999.

[11] A. Boglietti, S. Member, A. Cavagnino, and M. Lazzari, "Fast Method for the Iron Loss Prediction in Inverter-Fed Induction Motors", *IEEE Transactions on Industry Applications*, vol. 46, no. 2, pp. 806–811, 2010. DOI: 10.1109/TIA.2010.2040055.

[12] D. Graovac and M. Pürschel, "M O S F ET P o w e r L o s s e s Calculation Using the Data- Sheet Parameters", no. July, pp. 1–23, 2006.

[13] X. Liang, M. Luo, B. Zhao, Y. Yuan, and Z. Chen, "Research and implementation of SVPWM control algorithm based on FPGA", *2016 IEEE International*

Conference on Mechatronics and Automation, IEEE ICMA 2016, vol. 8, no. 100, pp. 22–26, 2016. DOI: 10.1109/ICMA.2016.7558528.

[14] A. M. Hava, S. Member, R. J. Kerkman, and T. A. Lipo, "A High-Performance Generalized Discontinous PWM Algorithm", *IEEE Transactions on Industry Applications*, vol. 34, no. 5, pp. 1059–1071, 1998.

[15] Adam, *Adam's Intelligence, "China's exports of ndfeb magnets increased 11% in 2018," February 2019.* 2018. [Online]. Available: https://www.adamasintel.com/china-ndfeb-exports-increased-2018/ (visited on 07/07/2019).

[16] T. E. Comission, *Reducing co2 emissions from passenger cars.* [Online]. Available: https://ec.europa.eu/clima/policies/transport/vehicles/cars%7B%5C_%7Den (visited on 07/07/2019).